

# Assessment of Process Modeling Tools for Determining Variability in Additively Manufactured Parts



Alex Plotkowski  
Gerry Knapp  
John Coleman  
Benjamin Stump  
Matt Rolchigo

**March 2023**

**M3CR-22OR0403042**



#### DOCUMENT AVAILABILITY

Reports produced after January 1, 1996, are generally available free via OSTI.GOV.

**Website:** [www.osti.gov/](http://www.osti.gov/)

Reports produced before January 1, 1996, may be purchased by members of the public from the following source:

National Technical Information Service  
5285 Port Royal Road  
Springfield, VA 22161  
**Telephone:** 703-605-6000 (1-800-553-6847)  
**TDD:** 703-487-4639  
**Fax:** 703-605-6900  
**E-mail:** [info@ntis.gov](mailto:info@ntis.gov)  
**Website:** <http://classic.ntis.gov/>

Reports are available to DOE employees, DOE contractors, Energy Technology Data Exchange representatives, and International Nuclear Information System representatives from the following source:

Office of Scientific and Technical Information  
PO Box 62  
Oak Ridge, TN 37831  
**Telephone:** 865-576-8401  
**Fax:** 865-576-5728  
**E-mail:** [report@osti.gov](mailto:report@osti.gov)  
**Website:** <https://www.osti.gov/>

This report was prepared as an account of work sponsored by an agency of the United States Government. Neither the United States Government nor any agency thereof, nor any of their employees, makes any warranty, express or implied, or assumes any legal liability or responsibility for the accuracy, completeness, or usefulness of any information, apparatus, product, or process disclosed, or represents that its use would not infringe privately owned rights. Reference herein to any specific commercial product, process, or service by trade name, trademark, manufacturer, or otherwise, does not necessarily constitute or imply its endorsement, recommendation, or favoring by the United States Government or any agency thereof. The views and opinions of authors expressed herein do not necessarily state or reflect those of the United States Government or any agency thereof.

Advanced Materials and Manufacturing Technologies Program

**Assessment of Process Modeling Tools for Determining Variability in Additively  
Manufactured Parts**

Alex Plotkowski

Gerry Knapp

John Coleman

Benjamin Stump

Matt Rolchigo

March 2023

M3CR-22OR0403042

Prepared by  
OAK RIDGE NATIONAL LABORATORY  
Oak Ridge, TN 37831  
managed by  
UT-Battelle LLC  
for the  
US DEPARTMENT OF ENERGY  
under contract DE-AC05-00OR22725



# CONTENTS

LIST OF FIGURES . . . . .	v
LIST OF TABLES . . . . .	vii
ABBREVIATIONS . . . . .	ix
ABSTRACT . . . . .	1
1. INTRODUCTION . . . . .	1
2. REQUIRED WORKFLOW COMPONENTS . . . . .	3
2.1 Process-structure-properties Relationships for SS316 Alloys . . . . .	3
2.2 Simulation Workflow . . . . .	3
2.3 Existing Modeling Workflows . . . . .	5
3. RESIDUAL STRESS AND DISTORTION . . . . .	7
3.1 Modeling Overview . . . . .	7
3.2 Heat Transfer Coarsening . . . . .	8
3.3 Constitutive Assumptions . . . . .	8
3.4 Inherent Strain Technique . . . . .	9
4. MELT POOL MODELS . . . . .	11
4.1 Analytical Melt Pool Models . . . . .	12
4.2 Numerical Melt Pool Models . . . . .	15
5. MICROSTRUCTURE MODELS . . . . .	18
5.1 Volume Averaged Methods . . . . .	19
5.2 Explicit Microstructure Modeling Methods: Sub-grain scale . . . . .	21
5.3 Explicit Microstructure Modeling Methods: Grain scale . . . . .	22
6. RECOMMENDATIONS FOR PROCESS MODELING DEVELOPMENTS FOR PREDICTING AM VARIABILITY . . . . .	24
6.1 Modeling and Methodology Improvements . . . . .	24
6.2 Workflow Opportunities . . . . .	25
6.3 Industrial Environment and Data Integration . . . . .	26
7. CONCLUSIONS . . . . .	28
8. REFERENCES . . . . .	29



## LIST OF FIGURES

1	LPBF SS316L after a creep rupture test at 650°C . . . . .	4
2	Coupling of physical phenomena that result in residual stresses during AM . . . . .	8
3	Length and time scales for thermal simulations relevant to predicting residual stress . . . . .	9
4	Examples of melt pool regimes during LPBF . . . . .	12
5	Comparison of computational expense for three general types of melt pool model . . . . .	13
6	Summary of the length scales for morphology-scale, grain-scale, and volume averaged solidification models. . . . .	19



## LIST OF TABLES

1	Summary of critical process-structure-property relationships for nuclear applications of powderbed fusion AM of SS316L. . . . .	5
2	Microstructural details resolved by modeling at different scales . . . . .	18



## ABBREVIATIONS

AI	Artificial intelligence
AM	Additive Manufacturing
AMMT	Advanced Materials and Manufacturing Technologies
BCC	Body-centered cubic
CA	Cellular automata
CALPHAD	Calculation of Phase Diagrams
CET	Columnar-to-equiaxed transition
DNN	Dendritic needle network
FCC	Face-centered cubic
G	Thermal gradient
GPU	Graphics processing unit
KGT	Kurz, Giovanola, and Trivedi
kMC	Kinetic Monte Carlo
LPBF	Laser Powder Bed Fusion
ML	Machine learning
NIST	National Institute of Standards and Technology
ORNL	Oak Ridge National Laboratory
PBF	Powder Bed Fusion
PDE	Partial differential equation
PF	Phase field
RVE	Representative volume element
SS316	Stainless Steel 316
V	Solidification velocity



## ABSTRACT

The Advanced Materials and Manufacturing Technologies (AMMT) [1] program aims to accelerate the development, qualification, demonstration, and deployment of advanced materials and manufacturing technologies to enable reliable and economical nuclear energy. However, the unique aspects of additive manufacturing (AM) materials in terms of their processing history, microstructure, and properties, are a major barrier for qualification and certification of nuclear components. Much of this challenge may be attributed to component scale variations in microstructure and properties that are driven by local influences of process conditions and geometry on thermal history, melt pool dynamics, and corresponding microstructure evolution. Computational modeling tools may be helpful in this regard to aid in predicting and controlling this level of variability. The purpose of this report is to review the current state-of-the-art for process modeling with regards to metal AM. For this purpose, we consider specifically the case study of laser powder bed fusion (LPBF) processing of SS316, a family of alloys that are both commonly used in nuclear energy applications and suitable for AM processing. The report first introduces the necessary components of a process modeling workflow, followed by a review of the current status of each. At the end, application of these modeling tools to understanding variability in AM process given their current state are considered, and recommendations for future development are proposed.

## 1. INTRODUCTION

Metal additive manufacturing (AM) processes offer complex geometries and unique material properties that might be beneficial for a variety of applications. For the nuclear energy industry, AM components may be capable of delivering superior performance and reduced lead times. However, despite the potential advantages, adoption of AM processing for nuclear energy applications has been a significant challenge, primarily driven by barriers for qualification and certification. Compared to conventional wrought processes, in which it is frequently assumed that material microstructure and properties may be considered uniform throughout a component, AM material often exhibits heterogeneous microstructures and properties that vary by location [2, 3]. These heterogeneities are a result of local thermal conditions in response to material deposition along the heat source path [4, 5, 6]. Because the pattern of material deposition is necessarily dictated by the programmed path of the heat source, there is an intimate link between the geometry of a component, the corresponding scan path, and resulting distribution of microstructure and properties. Therefore, a key challenge facing adoption of AM for nuclear component production is to understand the origins of microstructure and property variation, the physical phenomena that dictate the connection between processing, microstructure, geometry, and properties, and to predict and control the magnitude of variation and its effect on component performance.

Modeling and simulation tools of AM processes can offer insight into the relationships that control microstructure and property variability in AM [4]. Ideally, the physical phenomena may be simulated with sufficient predictive accuracy to predict distributions of thermal conditions, microstructure and defects. Furthermore, these models may complement experimental in-process data to act as a component of a "digital twin" that provides data to inform qualification and certification processes [7, 8]. The purpose of this report is to review the state-of-the-art for process modeling tools for AM and evaluate potential routes for providing information on relevant material variations that occur during processing. Ideally, these tools for process modeling may be connected in a unified workflow to predict the variation in microstructure in response to local variations in thermal conditions driven by process conditions and geometric variation.

In this report, we define process modeling as those things that occur during the AM process, including heat

and mass transfer in response to the moving heat source and the subsequent microstructure growth and transformations. The relevant physical phenomena frequently occur over length and time scales that span several orders of magnitude, from phenomena that occur within the melt pool to phenomena that occur at the component-scale [9]. Due to the significant variety of physical phenomena separated at the different scale, a single simulation tool is not capable of accomplishing all tasks required to assess process and material variability. Instead, a suite of tools must be identified, each selected to capture a particular set of phenomena at an appropriate scale. Furthermore, a recurring theme is the trade-off between physical fidelity of a given model and the computational expense. In all cases, models may be made more physical realistic by incorporating additional physics effects, but invariably, at the cost of additional complexity and expense.

For the purpose of describing relevant process modeling tools and approaches, explicit predictions of properties or component performance in service are not included in this report. However, the specific outputs that must be calculated by process models are discussed in the general context of nuclear applications of materials of interest. Because exact performance metrics are driven by specific application requirements, the most generally important process outcomes are determined and the physics needed to obtain the outputs from models are discussed. To limit the scope of this document to a specific example with potential near-term impact, we focus here on additive manufacturing of SS316 alloys, as they are both frequently used for nuclear energy applications, and are suitable for processing using AM technologies. Furthermore, the AM processing technology space is limited to laser powder bed fusion (LPBF) as it is the most common AM modality and is increasingly used for industrial applications.

Based on this framing, the report is structured as follows. First, the relevant process modeling workflow components are identified. The set of required simulation tools are based on a description of the relevant properties for nuclear energy applications, the associated microstructural features for SS316, and the anticipated physical processes that affect the formation of those features during processing. The subsequent sections focus on a review of the state-of-the-art for a range of relevant simulation applications, including residual stress and distortion, heat and mass transfer within AM melt pools, and microstructure evolution. Lastly, with considerations for potential near-term uses and the current status of simulation tools, recommendations are made for research and development to advance and incorporate process modeling to understand variation in AM SS316 components in response to process conditions and component geometry.

## 2. REQUIRED WORKFLOW COMPONENTS

Understanding material process-structure-property relationships, especially as they relate to material performance of PBF SS316 in nuclear applications, is necessary to determine process modeling workflow requirements. In this section, several aspects of the the performance of SS316 (and related stainless steel alloys) in nuclear applications are detailed from a literature review. Important material properties and microstructure features that determine performance are highlighted, and the the process model requirements for predicting these relevant features are addressed. Two particular variants of SS316 are considered: SS316H, a high carbon variant targeted for increased mechanical performance at elevated temperatures; and SS316L, a low carbon variant targeted for increased weldability and corrosion resistance.

### 2.1 PROCESS-STRUCTURE-PROPERTIES RELATIONSHIPS FOR SS316 ALLOYS

Stainless steel 316H is used for high-temperature nuclear applications mostly due to its increased creep resistance compared to SS316L at high temperatures and corrosion resistance [10]. Its use in high-temperature environments makes high-temperature strength, creep resistance, and phase stability important aspects of its performance. Additionally, SS316H's use in nuclear applications requires resistance to irradiation induced damage, such as irradiation creep, void swelling, irradiation hardening and embrittlement, and helium embrittlement. [10, 11, 12]. Other phenomena can also occur during irradiation, such as the agglomeration of vacancies into voids and dislocation loops in displacement damaged materials at high temperatures can result in irradiation-induced precipitate changes [13].

The material microstructure plays a significant role in determining the performance of a part. Under static loading, the grain size, sub-grain structure, and phase composition act to strengthen the material through Hall-Petch and precipitation strengthening. Stainless steel 316L has a unique solidification microstructure consisting of  $\delta$ -ferrite and  $\gamma$ -austenite when processed by LPBF due to the high solidification velocities [14]. Yoon et al. [15] show that during creep rupture tests of SS316L, cracks form along the ferrite-austenite grain boundaries near the melt pool boundaries (see Figure Figure 1).

Sub-grain microstructure features such as solute segregation, precipitation, and dislocation structures are also important. Klueh et al. [13] note that  $M_{23}C_6$  carbides help stabilize the lath boundaries in ferritic/martensitic steels and  $MX$  particles help pin dislocations. After exposure to high temperatures, these precipitates coarsen and can form Laves phase ( $(FeCr)_2(Mo, W)$ ). This is generally considered deleterious, though its formation does temporarily offset loss in strength during creep due to coarsening of the other precipitates.

Though austenitic stainless steels are generally more limited by creep resistance than oxidation and corrosion performance [16], there are several microstructure features that govern the corrosion performance. Chemical compatibility with the fuel, coolant, and structural materials that the steel will be in contact with is critical, as well as performance with regards to regular and irradiation-assisted stress corrosion cracking [10]. Additionally, the structure of the grain boundaries has been shown to influence the corrosion behavior in stainless steel 316L [17].

### 2.2 SIMULATION WORKFLOW

An outline of the process-structure-property relationships relevant for nuclear applications of austenitic stainless steel is provided in Table 1. The following list provides an overview of each section of the workflow diagram that is necessary to predict the relevant material structure and properties for a given

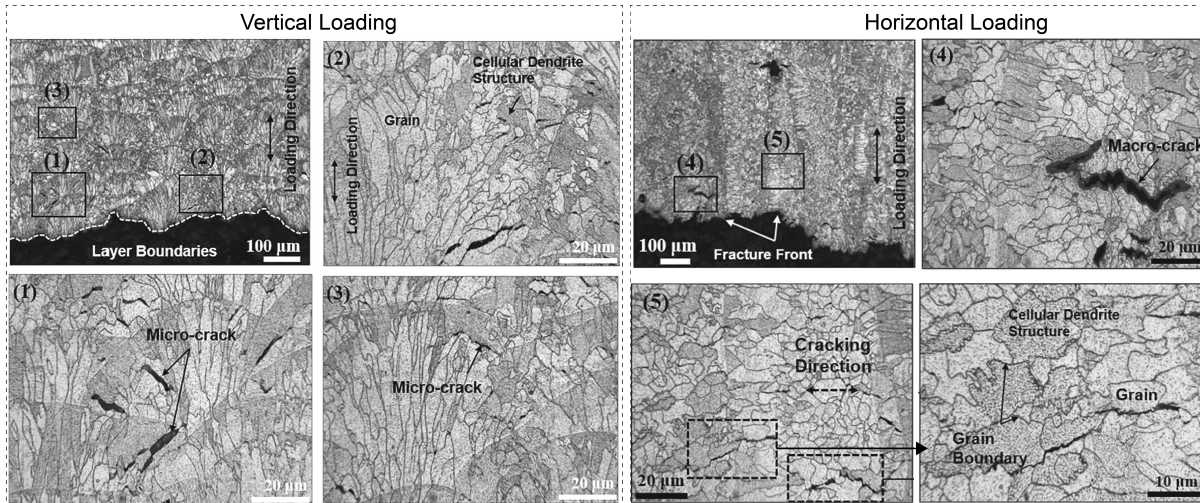


**Figure 1. LPBF SS316L after a creep rupture test at 650°C under the applied stress of 149 MPa in the vertical and horizontal orientations. Modified from Yoon et al. [15].**

application.

- **Process.** The laser powder bed fusion additive manufacturing process creates a part by repeatedly melting and solidifying a powder feedstock into some desired geometry. The outcomes of this layer-by-layer process are dependent on the powder feedstock properties [18], system settings such as laser beam properties [19] and gas flow [20], scan path parameters [21, 22], laser-material material interactions [19], solidification behavior, defect formation during processing [23], and post-process treatments [24].
- **Structure.** The structure of the manufactured material will depend on the processing route. In general, the performance of the structure is largely governed by microstructure features such as grain morphology, grain texture, residual stress, and grain sub-structures.
- **Properties and Performance.** The part properties are dependent on the structure that results from the processing of the material. The part performance is dependent on the interactions of the structure and properties of the material under various operating conditions. For example, the grain morphology influences the location of helium porosity that can form during operation, which influences the mechanical properties and failure mode of the material. Corrosion, precipitation, and phase decomposition also depend on the structure of the material and the operating conditions of the part.

Before a specific modeling workflow can be established to predict properties and performance of SS316 alloys in nuclear applications, relevant material and processing characteristics related performance must be identified. Almost all the properties important to SS316 performance in nuclear application are related to the microstructure grain size, grain morphology, and sub-grain morphology. Therefore, a critical component of a process model for LPBF SS316 is the ability to output representative grain structures for different regions of the part. The microstructure of LPBF materials arises from the solidification and solid-state thermal cycling that occur during processing, meaning that the heat transfer conditions in and around the melt pool must be considered. Moreover, the solidification of the material is driven by the

interaction of local thermal conditions and the material’s thermodynamic and kinetic properties, requiring the use of a representative solidification model. After the material solidifies, solid-state phenomena, such as residual stress and solid-state phase transformations, further lead to changes in the microstructure of the material that must be considered. Existing workflows that capture many of these requirements will be discussed subsequently, followed by more detailed discussion on state of the art modeling tools developed for individual components of a process modeling workflow, namely: melt pool and heat transfer models, microstructure models, and residual stress models.

**Table 1. Summary of critical process-structure-property relationships for nuclear applications of powderbed fusion AM of SS316L.**

<b>Process</b>	
<i>Material Properties</i>	<i>Machine and Post-processing</i>
Powder feedstock morphology Material solidification behavior Thermophysical properties	PBF system parameters Defects (spatter and porosity) Heat treatment

<b>Structure</b>				<b>Properties and Performance</b>
<i>Grain structure</i>	<i>Grain texture</i>	<i>Sub-grain structure</i>	<i>Residual Stress</i>	
X	X	X	X	<i>Mechanical strength/failure</i>
X	X			<i>High-temperature creep deformation</i>
X				<i>Helium embrittlement</i>
X		X	X	<i>High-temperature phase stability</i>
X	X	X	X	<i>Corrosion</i>

### 2.3 EXISTING MODELING WORKFLOWS

In the past decade, improvements in powder bed fusion model implementations and process understanding have allowed for models to move from disparate representations of individual components of the process [25, 26] towards models that bridge multiple length and time scales to capture process-structure-property relationships [27, 4, 28, 29]. This transition was partially enabled by concerted efforts within the AM modeling community to develop robust multi-physics models for AM processes. Experimental datasets that revealed data-driven insights and could be used as validation of individual components of multi-model workflows were critical to progress. Experimental data includes some highly pedigreed data, such as the AM Bench 2018 and 2022 benchmarks published by NIST [30]. While there is not a current standard for model validation, benchmark data is a necessity for development of such standards [31].

In a recent review of multi-scale model capabilities and workflows for additive manufacturing by Bayat et al. [27], the coupling between modeling length scales was identified as a critical component of developing modeling workflows for AM processes. Wei et al. [4] conclude that one method to address this is by developing reasonably accurate coarse scale models to capture the most important effects during processing. Regardless of the approach, multiple models must be developed and coupled to compute, at the very least, the AM process heat transfer, solidification, and grain solidification. Because of the need to couple multiple models, the communication and data transfer between models becomes a challenge. For example, a reduced data format for communicating data from a heat transfer model to a cellular automata model for solidification grain growth had to be developed to avoid needing to transfer the entire

temperature field between models [32]. Similar challenges exist when creating an interface between any two models. An additional challenge is that while it is possible to manually transfer data between models, the development of automated workflows between codes is critical to making modeling workflows useful tools for process design and engineering in addition to being scientific research tools. Aspects of these challenges are beginning to be overcome, as demonstrated by some examples of multi-scale workflows connecting the process-structure-properties of materials [28, 29]. However, it should be noted that these workflows are computationally intensive and currently not easily extended to investigate large numbers of parts or process conditions without using large amounts of high-performance computing resources. Once the model development challenges are completed, the work of Turner et al. [28] and Bierwisch et al. [29] highlight that the importance of model validation both at the level of individual models and the overall workflow.

Model validation requires experimental data, so running experiments or extracting literature data is also an important part of the modeling workflow. If data collection and storage is done in a systematic way, data-driven approaches to better digitize, store, and make predictions from existing and newly generated experimental data are also enabled, in addition to physics-based modeling. Scime et al. [33, 34] have developed a digital factory tool set that enables *in situ* data from the AM systems to be stored and analyzed in a digital ecosystem. As such tools are adopted, a rich dataset of AM build data and part properties will enable increasingly rigorous model validation and incorporation of model-generated features into the digital representation of a part, *i.e.*, a digital twin [7, 8]. Even with limited experimental data, at least compared to the typical sizes of datasets considered in data science applications, data-driven approaches are being taken to make property predictions. Machine learning approaches have been used to leverage experimental data, which is often noisy, and combine it with a mechanistic understanding of the process [35], such as linking *in situ* thermal data to mechanical properties [36] or melt pool characteristics to defects [37].

Overall, there are examples of existing workflows that can simulate the LPBF AM process and resulting microstructure features. These tools could be used to inform process parameter development for achieving desirable microstructure traits for nuclear application, if it is possible to close gaps in the ability to run these model workflows automatically and in a timely manner while using reasonable amounts of computational resources. The purpose of the remaining portion of this report is to capture the current state-of-the-art for these workflow components, and then to consider how they may be connected into an overall workflow to specifically address challenges in microstructure and property variation in LPBF SS316 components.

### **3. RESIDUAL STRESS AND DISTORTION**

Residual stress is a type of stress which remains in a material even after removing the cause of the original stress and is a common phenomenon found in material processing. In materials processing, residual stress results from the gradient in the plastic strain field within a material which itself can change during mechanical processing, phase transformations, and in regions with high thermal gradients [38].

Additive manufacturing PBF processes are known to have large thermal gradients near the heat source which will induce stresses and strains due to the spatially varying thermal expansion within the printed material. Since these thermal gradients are so large, the resulting stresses cannot be accommodated by an appropriate elastic strain field and thus results in plastic strain as well [39]. The resulting residual stress can lead to a variety of challenges. Since residual stress must be balanced in the object, the amount of tensile (positive) stress must be compensated by an equal amount of compressive (negative) stress causing distortion. For example, a component may distort in place during a build or upon the redistribution of stresses when it is removed from the build plate, causing challenges in maintaining geometric accuracy. If not annealed, residual stress distributions within a component may also affect performance, such as fatigue crack initiation and propagation [40], or stress corrosion cracking [41].

The ability to model residual stress is important for producing repeatable components that meet expected geometric tolerances, for determining effective post-processing heat treatments and machining strategies, and to ensure consistent properties and performance. Effective prediction of residual stress requires some consideration for the thermal evolution of the process in response to the part geometry, a constitutive model of the material behavior which is in turn dependent on microstructure evolution and thermal conditions, and a mechanical model of the stress evolution [42]. Figure 2 shows the various relationships and interactions that dictate eventual residual stress distributions.

#### **3.1 MODELING OVERVIEW**

In many ways, modeling residual stress in AM is similar to that of in welding, and indeed, many researchers in this area for AM have pulled heavily from the decades long history of computational weld mechanics [43]; however, there are also key differences between modeling residual stress in these two fabrication processes, the primary concern being computational efficiency. Fabrication of AM components is done using numerous welds, thus the computational challenge increases by orders of magnitude associated with the scale of the component and process conditions. Because residual stress is linked to thermal stresses that occur during processing, some prediction of the thermal fields induced during the process is necessary. Thermal stresses may then evolve based on the coefficient of thermal expansion of the material, energy input, and both the thermal and mechanical boundary conditions. Calculation of the material response then requires a description of the constitutive mechanical behavior of the material as a function of temperature. Naively linking the entire thermomechanical response at the component scale is prohibitively expensive since the length and time scales needed for resolving the energy input are miniscule compared to those of the process. It is therefore necessary to make certain sets of assumptions or simplifications to enable computational efficiency adequate for component scale simulations. The models used for these simulations can be broadly classified based upon the types of assumptions they invoke regarding the thermal and mechanical effects of the process and material.

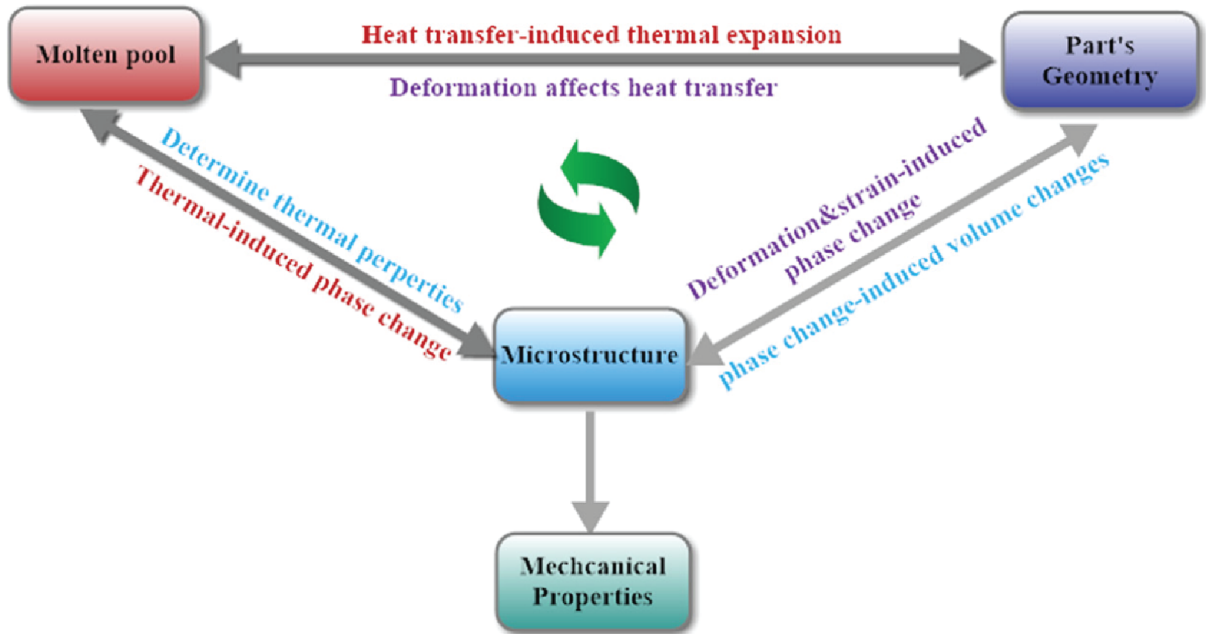


Figure 2. Coupling of physical phenomena that result in residual stresses during AM [44].

### 3.2 HEAT TRANSFER COARSENING

Because the scale of the component is large compared to that of the melt pool, simplifications of the heat transfer behavior are often applied to accelerate simulation times, even extending to cases where the simulation elements are large compared to the AM layer thickness. Figure 3 shows a range of relevant thermal models for the purposes of residual stress predictions arranged by their approximate length and time scales [45]. At the lowest length and time scale, the physics of the melt pool may be considered explicitly. Although this may be relevant for solid deformation very close to the melt pool, these effects are frequently neglected for the purposes of part scale residual stress prediction to save computational expense. At intermediate length and times scales, the melt pool itself is simplified while still explicitly considering the movement of a heat source throughout an individual layer. At the highest scales the movement of a heat source within layers is neglected with the energy content for full layers or even groups of layers being at a single time [46].

### 3.3 CONSTITUTIVE ASSUMPTIONS

For stress evolution, the most physically realistic simulations use coupled thermomechanical models that include the heat transfer, thermal expansion, and elastic-plastic constitutive materials behavior. These simulations generally rely on finite element frameworks to capture thermally induced stresses in response to thermal expansion and the coupled material deformation behavior. The computational expense of these models is dependent upon both length scale and the complexity of the constitutive material model. At a minimum, temperature dependent elastic and plastic deformation must be captured to reasonably estimate final residual stresses. However, in many cases it is also necessary to capture strain-rate effects as a function of temperature. This effect may be captured by viscoplastic models, but at significant

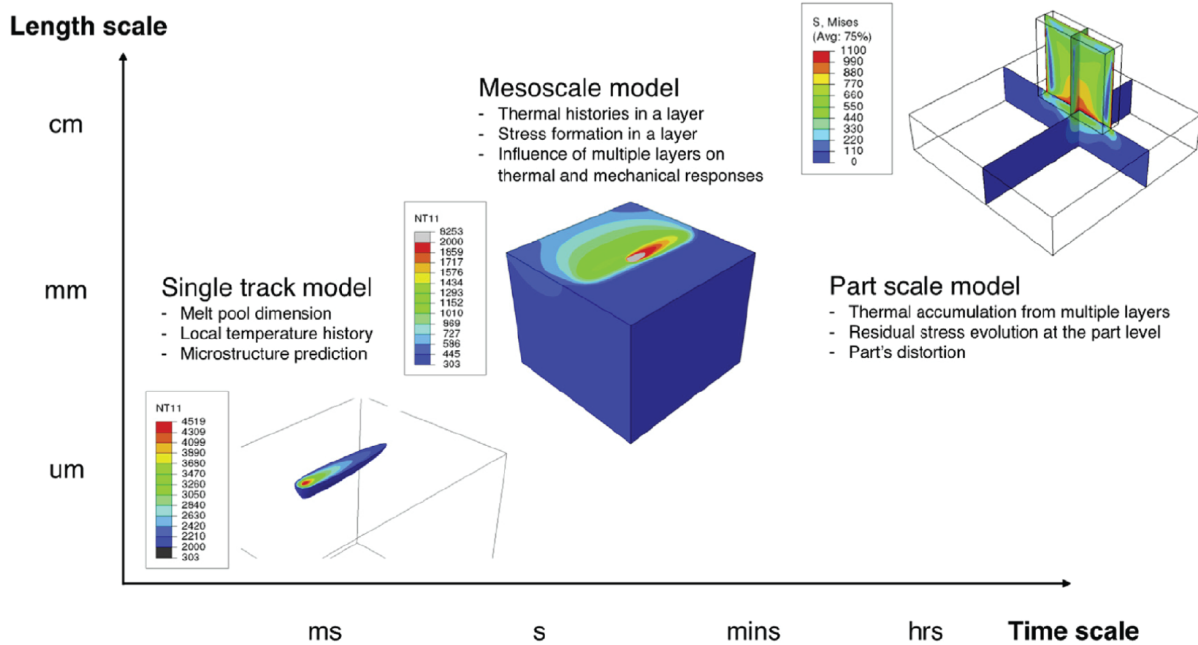


**Figure 3. Length and time scales for thermal simulations relevant to predicting residual stress [45].**

computational expense. Ganeriwala et al. [47] compromised between these trade-offs by following Goldak [48] in implementing multiple models each active in a restricted temperature range, allowing for strain-rate independence at low temperatures ( $T < 0.5T_m$ ), viscoplasticity at intermediate temperatures ( $0.5T_m < T < 0.8T_m$ ), and Maxwell type viscoplasticity at high temperatures ( $T > 0.8T_m$ ).

### 3.4 INHERENT STRAIN TECHNIQUE

Coupled thermomechanical simulations tend to be computationally intensive, requiring large computational resources and scalable algorithms such as adaptive mesh refinement [49]; however, for most practical situations, coupled thermomechanical models are too computationally intensive for regular use at the part scale. A common approach to simplifying and accelerating the simulations, originally developed for welding [50], is to assume an initial eigenstrain for newly deposited material, also referred as an "inherent strain", which may then relax to develop the final residual stress distribution. More recently, the inherent strain technique and extensions of it have been adopted by a variety of researchers to investigate residual stresses in AM [51, 52, 53, 54, 55]. This family of approaches has the advantage of being significantly less computationally intensive than complete coupled simulation of the thermomechanical response and accumulation of plastic strains [56] although the eigenstrain with which each newly added element is initialized behaves as a calibration parameter. Properly calibrated inherent strain models are capable of reasonable predictions for residual stress distributions but it is unclear whether these calibrations are transferable between different build conditions, for example, different geometries or process conditions. Indeed, Bugatti and Semeraro [57] found that while calibration of the initial eigenstrain within a specific geometry gave excellent prediction across the rest of that same component, predictions for another geometry were poor by comparison.

The challenge of setting an appropriate initial eigenvalue for new elements with the inherent strain technique places an emphasis on the approach to model calibration. Initial work on calibrating the inherent strain during welding relied on experimental measurements of final residual stress distributions using x-ray or neutron diffraction techniques [50]. For AM, inherent strain techniques have been calibrated against the distortion observed in cantilever beam samples following careful sectioning from the build plate [58]. Alternatively, a full thermomechanical simulation may be performed as a sub-model on a representative portion of the domain to directly estimate the eigenstrain values that can be used as input for the inherent strain method [51]. Li and Anand [59] used a series of coupled thermomechanical simulations to train a neural network to estimate the appropriate inherent strain.

## 4. MELT POOL MODELS

The solidification characteristics of the melt pool during AM process determines the solidification microstructure, a key factor in the properties and performance of LPBF SS316. Solidification is dependent on the transport of heat from the melt pool to the surrounding areas; therefore, simulation of the heat transfer during the PBF process can provide data for microstructure simulations and insight into the origin of as-built microstructure. These models can consider numerous physical phenomena that occur during processing, including but not limited to laser-material interactions, temperature-dependent thermophysical properties of material, and multi-phase flow. This section will discuss important melt pool physics and the modeling approaches generally used to simulate the melt pool for PBF processes [25, 4].

Melt pools as characterized in the welding literature are typically classified as either conduction-limited mode (a.k.a. conduction mode), keyhole mode, or transition mode. Often these modes are determined by ex situ characterization of the transverse melt pool cross-section as shown in Figure 4. In Figure 4, the depth and aspect ratio of the melt pool vary drastically as a function of process parameters (in this case, spot size). The characteristics and rationale for the formation of these modes are detailed in a recent review on the topic [19] and can be summarized as follows:

- **Conduction mode:** The extent of melting is limited by conduction of heat into the substrate. This limits the temperature of the melt pool to be mostly below the vaporization temperature (a small amount of localized boiling and a small vapor cavity may occur near the center of the heat source [60]). Surface deformation is generally minimal and mostly driven by surface tension effects. Due to the relatively flat surface, the laser reflects once off the surface of the melt pool, making the total absorption equal to the Fresnel absorption. Melt pools typically have shallow depths, less than the half-width of the melt pool.
- **Transition mode:** The heat flux into the melt pool from the laser begins to overcome the heat flux out of the melt pool due to conduction into the substrate. Temperatures in the melt pool begin to reach the boiling point of the alloy and some vaporization occurs. The recoil force from the vaporization depresses the surface of the melt pool and the effective absorption of the laser is increased due to a small number of multiple reflections that occur due to the surface depression. The melt pool depth is generally equal to or slightly deeper than the melt pool half-width.
- **Keyhole mode:** The temperatures of the melt pool surface beneath the laser is almost entirely at the boiling point and significant depression of the melt pool surface is observed. Due to the deep depression of the melt pool surface, the total energy absorbed by the laser increases due to a significant number of multiple reflections. The melt pool depth is deeper than the melt pool half-width.

Due to the complex physics involved in the heat and mass transport of the melt pool, especially in the transition and keyhole melting modes, there are numerous approaches to modeling the melt pool. Modeling the thermal conditions in the vicinity of AM melt pools can be done at various levels of physical fidelity, with the higher fidelity models including a greater number of physical phenomena while also incurring higher computational burdens. A continuum mixture formulation of the energy conservation equation during AM processing can be defined in terms of temperature according to:

$$\frac{\partial(\rho c_p T)}{\partial t} + \nabla \cdot (\rho c_p u T) = \nabla \cdot (k \nabla T) + L_f \frac{\partial(\rho_s f_s)}{\partial t} + \dot{Q}(t) \quad (1)$$

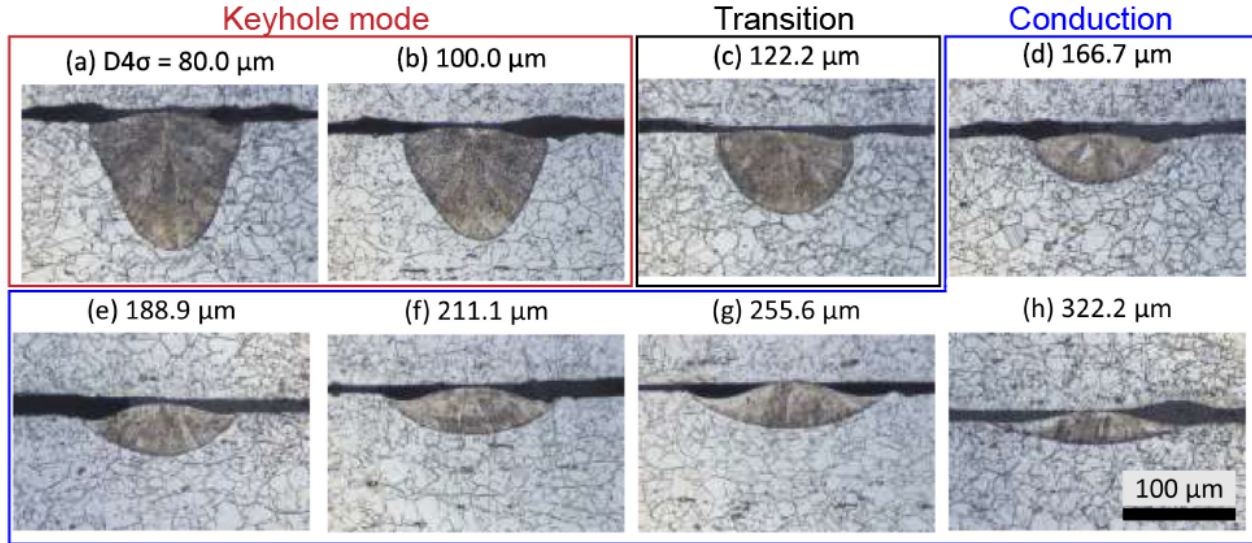


**Figure 4. Examples of (a-b) keyhole, (c) transition, and (d-h) conduction mode melt pools. Adapted from Weaver et al. [61]**

where  $\rho$  is density,  $\rho_s$  is the density of the solid in the mushy zone,  $c_p$  is specific heat,  $T$  is temperature,  $t$  is time,  $u$  is fluid velocity,  $k$  is thermal conductivity,  $L_f$  is latent heat, and  $f_s$  is the solid mass fraction. Briefly, Eqn. 1 describes the balance between the storage and advection of heat (left-hand side of 1), with the conduction, latent heat evolution during phase change, and heating from a moving laser (right-hand side of 1). The solution to the temperature field can be calculated at various length and time scales across AM processes, including the part scale (macroscopic), the melt pool scale (mesoscopic), and the powder scale or smaller (microscopic). The following sections are focused on the usage and trade-off between different solution methods employed to resolve the heat and mass transport at the melt pool scale. In general, two different approaches are often used. The first approach uses (semi)-analytical methods that are fast and computationally efficient, but do not consider nonlinear effects and or the explicit system geometry. The second approach uses numerical methods which are more flexible in terms of the fidelity of included physics, but are often much slower than the (semi)-analytical approaches. A comparison of the fidelity and computational expense for these types of melt pool models is provided in Figure 5.

#### 4.1 ANALYTICAL MELT POOL MODELS

The lowest fidelity melt pool modeling is performed by a) considering only linear heat conduction and b) considering a semi-infinite domain, which reduces equation 1 to equation 2:

$$\rho c_p \frac{\partial T}{\partial t} = k \nabla^2 T + \dot{Q}(t) \quad (2)$$

Under the stated assumptions, the solution to 2 becomes analytically tractable for several definition of the heat source,  $\dot{Q}(t)$ . Several examples of analytical melt pool models are presented in this section.

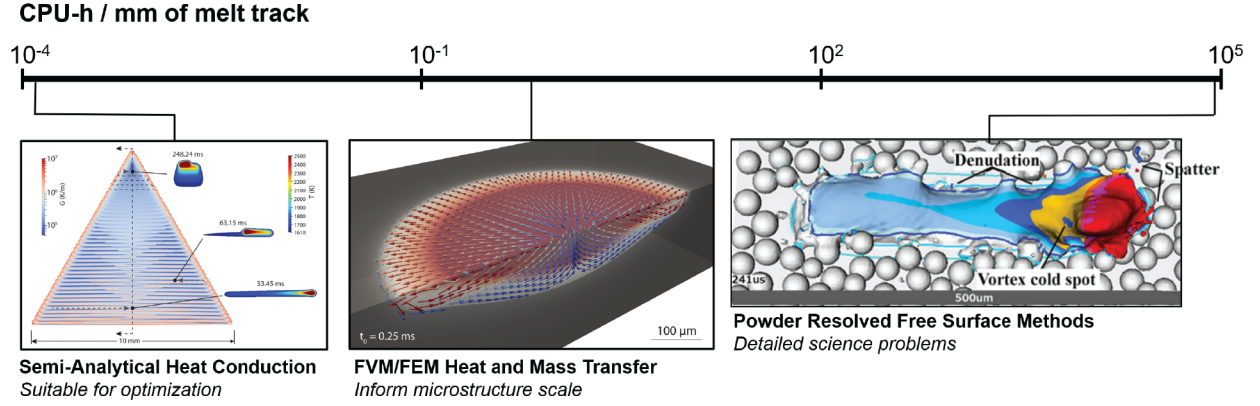


**Figure 5. Comparison of computational expense (given as CPU-h / mm of melt track) for three general types of melt pool model, including semi-analytical approaches [62], continuum numerical models [63] and free-surface resolved models [64]**

The Rosenthal solution provides a quasi-static solution to the temperature field from the reference frame of a point heat source moving at a constant velocity [65].

$$T(x, R) = T_0 + \frac{\dot{Q}}{2\pi k} \frac{e^{-\frac{v}{2\alpha}(x+R)}}{R} \quad (3)$$

$$\alpha = \frac{k}{\rho c_p}$$

where the heat source is moving in direction  $x$  with velocity  $v$ ,  $R$  is in the direction perpendicular to the moving heat source in a cylindrical coordinate system, and a constant temperature  $T_0$  is maintained far from the top surface. Despite the simplicity of the Rosenthal solution, the predicted melt pool geometry and thermal conditions has been used to justify both lack-of-fusion porosity [66] and grain morphology [67].

Later, the multi-pass welding community derived a variety of solutions for the transient thermal distribution around moving heat sources, breaking down the assumption of quasi-steady state used in the Rosenthal solution. For example, Eagar and Tsai used a Green's function approach to derive the temperature distribution around a moving Gaussian surface heat flux [68]. As representative of this type of approach, we present here the solution by Nguyen [69] to the transient thermal field around an arbitrarily moving volumetric Gaussian heat source, defined by the set of position functions  $\{x(t), y(t), z(t)\}$  and the set of shape parameters  $\{\sigma_x, \sigma_y, \sigma_z\}$  :

$$\dot{Q}(t) = 2\eta P e^{-3 \left[ \frac{\Delta x(t)^2}{\sigma_x^2} + \frac{\Delta y(t)^2}{\sigma_y^2} + \frac{\Delta z(t)^2}{\sigma_z^2} \right]} \frac{1}{\sigma_x \sigma_y \sigma_z (\pi/3)^{3/2}} \quad (4)$$

$$T(t) = T_0 + \frac{2\eta\dot{Q}}{\rho c(\frac{\pi}{3})^{\frac{3}{2}}} \int_0^t (\phi_x\phi_y\phi_z)^{-\frac{1}{2}} e^{-3\left[\frac{x(t')^2}{\phi_x} + \frac{y(t')^2}{\phi_y} + \frac{z(t')^2}{\phi_z}\right]} dt' \quad (5)$$

$$\phi_i = 12\alpha(t - t') + \sigma_i^2$$

$$i = x, y, z$$

Other similar solutions for different heat source shapes may be derived, the effect of which modifies the form of the integrand and the pre-integral factor. Because of the piece-wise nature of the scan path description, the integral in Eq. 5 needs to be computed numerically. The computational cost is therefore directly related to the speed and scalability of the integration technique. Forslund's integration technique [70] uses a lookup table to determine the quadrature order for each piece-wise segment of a scan path. Schwabach's integration technique [71] explicitly ignores the contributions from heat sources that are determined to be sufficiently far away in space-time, such that their impact on the temperature at any given point in space-time are negligible. Finally, Stump [62] uses an adaptive integration technique to gradually reduce the quadrature order while simultaneously increasing the integration segment size as the nondimensional diffusion time increases.

A major advantage of analytic solutions over numerical solutions is that each point in space-time can be calculated independently, which allows for further reduction of the computational load depending on desired outputs. Some examples include: melt pool tracking, which calculates only liquid points [62]; spatiotemporal decomposition [72], which improves the scalability of the solution by calculating points on separate computing resources in parallel; and the ability to calculate only points in a cross-section or subregion of an entire build. These features of analytical solutions can dramatically reduce the computational resources required for AM simulations by either reducing the number of dedicated processors or improving scalability on distributed computing architectures.

There are several prominent examples where the speed and scalability of semi-analytical solutions are leveraged to simulate significant regions of AM builds. Donegan [73] uses a zoning procedure based on the simulated thermal histories to successfully separate different regions and allow for comparisons between geometries. Raghavan [2] simulates both the final surface temperature field, which strongly correlates to the surface finish observed via microscope, as well as the bulk solidification gradients and velocities, which were correlated to the observed microstructure. Kamat [74] uses the simulated thermal histories from a high-resolution subsection of a larger build for microstructural prediction via cellular automata (CA), which share many morphological characteristics with the experimental results.

Additionally, the speed and scalability of semi-analytical solutions has been leveraged for process optimization of AM builds. Halsey [75] uses a genetic algorithm to adjust point order and spot time to control simulated surface solidification conditions. Plotkowski [5] developed a novel scan pattern design whose hyper-parameters were iteratively adjusted via simulation of the top surface. The resulting scan pattern resulted in distinct micro-structural regions depicting the Mona Lisa in an as-built part. Ogoke [76] utilizes deep reinforcement learning to alter either the power or velocity to maintain a constant simulated melt pool depth along predefined paths. Stump [77] combines a convolutional neural network with a semi-analytic model to iteratively determine point order and spot times to control simulated bulk solidification conditions. Finally, Yang [78] makes slight adjustments to predefined paths and dynamically changes scan speed to give desired distributions for the maximum temperature at select points.

Despite lacking many relevant physical phenomena found in AM, analytic melt pool models have been

shown to be accurate wherever the assumptions used to make the heat transfer solution analytically tractable are valid; specifically, in the conduction regime, where the diffusion of heat away from the moving heat source dominates the overall heat transfer near the melt pool. Stump [79] shows that the parameters describing the heat source shape in a semi-analytical model can be calibrated against melt pool geometries predicted using higher-fidelity models in the conduction regime. When this calibration is performed, the solidification conditions are similar for both models, differing mainly near the melt pool tail where the diffusion of latent heat through the mushy zone is limited. This difference in solidification conditions can be corrected with a posterior correction factor. Similarly, Khorasani [80] compared the melt pool temperatures predicted using a analytic solution to a high-fidelity powder-resolved model, and showed that the simple analytic solution only becomes inaccurate once a keyhole begins to form.

## 4.2 NUMERICAL MELT POOL MODELS

Numerical models numerically discretize and solve the partial differential equations (PDEs) describing the heat and/or mass transport in time and space. Because numerical models arrive at a mathematically approximate rather than a mathematically exact solution to the governing PDEs, these models can consider a much wider range of possible physical phenomena in AM compared to the analytical and semi-analytical models described in the previous section. In general, these numerical models represent and evaluate PDEs in the form of algebraic equations, which is achieved by subdividing the system into either finite volumes or finite elements. The advantages of including an accurate representation of complex geometries and the selection of relevant physical phenomena come at the expense of significant code development overhead such as meshing libraries to subdivide the system into volumes or elements, and linear algebra libraries to solve the resulting set of algebraic equations in a performant and stable manner. For these reasons, numerical AM models are generally implemented as specific applications within larger finite volume frameworks such as OpenFOAM [81], or finite element frameworks such as deal.ii [82].

There are several prominent examples where numerical models have been successfully adapted to predicting both the melt pool- and part- scale transport phenomena in AM. Starting at the simplest implementation, numerical melt pool models may consider non-linear heat conduction in which effects such as temperature dependent properties, latent heat evolution, and complex boundary conditions may be included. In these cases, the highly non-linear effect of the latent heat release in the thin mushy zone is frequently the limiting factor determining mesh resolution and stable time step to achieve accurate solutions. Such solutions may be considered a reasonable extension of the semi-analytical models listed in the previous section, but able to better capture the physics of the solidification behavior and the effect of component scale boundary effects [79]. These models are generally called continuum or macroscopic models, because they do not resolve individual powder particles or mass transport due to fluid flow.

A major advantage to numerical melt pool models is that they may solve coupled PDEs that do not have exact solutions to incorporate the complex fluid dynamics that occur in the liquid metal. These effects are primarily driven by Marangoni effects, i.e., differential surface tension forces caused by strong thermal gradients at the liquid-vapor interface [83]. The treatment of this interface has a significant effect on the computational complexity and expense of the corresponding model, and may be used to broadly classify different approaches. The most straightforward assumption that is frequently invoked is that the liquid-vapor interface may be considered flat and coincident with a boundary of the numerical domain. In this approach, the component of the temperature gradient tangential to this boundary may be used to calculate a shear force boundary condition for the momentum equation that drives fluid flow within the

melt pool, such that :

$$\mu \frac{\partial u}{\partial n} = \frac{\partial \gamma}{\partial T} \frac{\partial T}{\partial \tau} \quad (6)$$

where  $\mu$  is the dynamic viscosity of the fluid,  $n$  is the normal vector to the boundary,  $\partial\gamma/\partial T$  is gradient of the surface tension with respect to temperature, and  $\partial T/\partial\tau$  is the component of the temperature gradient tangential to the surface. Coleman [63] showed that this simplified treatment of Marangoni convection produced accurate predictions of the melt pool shape across a range of processing parameters in the conduction regime (i.e. no keyhole formation), provided that the correct value of the surface tension gradient was used.

As a keyhole begins to form, the assumption that liquid-vapor interface remains coincident with a flat boundary begins to misrepresent the both the orientation and magnitude of the Marangoni forces and more complex and expensive models must be used to better represent flow conditions driven by a free surface. In these models, the evolution of the liquid-vapor interface is explicitly calculated, for example, using the volume-of-fluid technique in the finite volume framework or the level-set method in the finite element framework. These approaches allow for further inclusion of complex physics associated with the liquid-vapor interface such as free surface deformation, elemental vaporization, recoil pressure, laser and powder interactions with the free surface and vapor, and keyhole formation. Inclusion of these free surface models into melt pool models of AM comes at a significant computational burden. In addition to the cost associated with interface reconstruction techniques, the spatiotemporal resolution needed to resolve the local curvature of the liquid-vapor is about 5-10x finer than simulations where this interface is not considered. Therefore, these free surface models are generally limited to simulating only a few millimeters of tack in the LPBF process.

Nevertheless, several of these free-surface evolution have been successfully used to gain insight into the complex dynamics governing LPBF processes. Matthews et al. [84] used one such model to show that gas flow due to vaporization in the vicinity of the melt pool tends to entrain local powder particles and create a denuded zone surrounding the melt track. A variety of researchers, including Wang et al. [85] and [86] have used free-surface resolved models to study the dynamics of keyhole formation and instability leading to porosity as a function of process conditions. Other studies have investigated the interaction of the heat source and melt pool with the surrounding powder particles [87, 88] or used ray tracing techniques to understand the effective absorption of the heat source by the melt pool and surrounding material [89, 90].

A major challenge with any AM model considering fluid flow in the melt pool stems from the significant uncertainty in the necessary model inputs. In particular, the evaluation of the surface tension as a function of temperature at the liquid-vapor interface is a necessary step for accurately estimating the direction and magnitude of the Marangoni forces. Unfortunately, surface tension for liquid metals at elevated temperatures is both extremely challenging to measure experimentally and highly sensitive to small changes in composition and surface conditions. Experimental measurement generally involves electrostatic levitation of liquid metal droplets, the vibratory frequency of which may be used to extract surface tension information [91]. A study by the welding community has established that the Marangoni forces and resulting melt pool shape may be highly sensitive to small impurity levels of so called "surface active elements" such as oxygen [92] and sulfur [93, 94] that affect the surface tension gradient with respect to temperature. Consequently, it has been acknowledged that accurate determination of surface tension gradients as a model input is highly uncertain and may not even be transferable between material batches [91]. Frequently, the exact value of the surface tension term is therefore calibrated by matching predicted melt pool shapes to ex-situ metallographic cross-sections (e.g., [63]).

Owing to the uncertainty in accurately modeling fluid flow in AM melt pool models, it is important to understand its relative importance in controlling the melt pool shape in terms of processing conditions. The competition between the advection and conduction of heat on the length scale of the melt pool is described by the non-dimensional Peclet number:

$$Pe_c = \frac{u_c w}{2\alpha} \quad (7)$$

where  $u_c$  is the characteristic velocity within the melt pool,  $w$  is a characteristic length, generally taken as the melt pool width, and  $\alpha$  is the thermal diffusivity. In general,  $Pe_c$  values greater than one indicate an advection dominated regime, whereas values less than one indicate a conduction dominated regime. The interpretation of  $Pe_c$  depends on the selection of the characteristic velocity. Frequently, the maximum fluid velocity within the melt pool is used [95]. Because the largest thermal gradients driving flow are close to the center of the heat source, the maximum velocity is localized within a small portion of the melt pool. This form of  $Pe_c$  is therefore relevant for localized effects such as elemental vaporization. However, Coleman et al. [63] found that using the average fluid velocity to describe the behavior of the melt pool correlated better with experimental observations of the deviation of melt pool profiles from the conduction dominated regime.

With this insight, it is possible to consider various regimes of behavior. For applications such as arc welding or directed energy deposition processes, it is common to use high power energy sources (>kW) with large effective spot size (>1mm) and relatively low traverse rates (mm/min). In these cases, the melt pool width  $w$  is large and the flow velocity is anticipated to be high, as the heat input is large, with correspondingly large thermal gradients and Marangoni forces. In these cases,  $Pe_c$  is expected to be comparatively large, and fluid flow plays an important role in determining the melt pool shape and characteristics such as elemental vaporization. However, in LPBF processing, comparatively low power (100-1000 W) lasers with small spot sizes (80-500  $\mu m$ ) and high scan velocities (> 1 m/s) tend to be used. In these cases, the melt pools are small, and fluid flow does not necessarily play as dominant a role.

Given the uncertainty in many parameters governing fluid behavior in the melt pool and the computational cost associated with its computation, an alternate approach has been to design and calibrate effective heat source models in conduction based models to approximate the effect of fluid flow and keyhole formation on the melt pool shape. This approach may be considered reasonable given the discussion above for cases in which  $Pe_c$  is close to or below one. In these regimes, characteristic of many LPBF processing conditions, an effective heat source shape may be able to accurately consider slight deviations from conduction dominated behavior to improve prediction of melt pool shapes without incurring the expense of solving the momentum conservation equations or including explicit description and tracking of the free surface. For example, Knapp et al. [96] showed that using an automated calibration technique, it was possible to achieve similar levels of agreement using an effective heat source model in a conduction only simulation with consideration of Marangoni driven fluid flow. Both types of simulation were used to drive a CA-based grain structure model, and equivalent microstructures were achieved.

## 5. MICROSTRUCTURE MODELS

Determining variability of component performance as a result of AM processing requires an understanding of the linkages between microstructure and properties, and therefore, first an understanding of the evolution of the relevant microstructural features. In the case of SS316 alloys, the grain structure is of primary importance. This microstructure forms as a consequence of the behavior locally during solidification, resulting in the formation of dendrites, and their nucleation, growth and competition, and the effects of these phenomena on development of the overall grain structure. Features of interest include quantities such as the distribution of grain size, aspect ratio, and crystallographic texture. Because the formation of the grain structure is governed by the short length scale evolution at the solid-liquid interface, microstructural models must consider the mesoscale behavior that connects the melt pool scale to the physical phenomena governing microstructure development.

Mesoscale modeling methods for the microstructure formed during alloy solidification, and the comparison of the various available methods, has been the subject of several recent review articles [97, 98, 99, 100, 101, 102]. In general, the methods fall into one of three categories: volume averaged methods, sub-grain (or morphology) scale methods, and grain-scale methods. Methods from a given category output similar quantities with increasingly detailed representation of a microstructure and a corresponding increase in computational cost as various details of the problem are considered explicitly. Figure 6 graphically illustrates the scales and computational expense of some of these methods, while 2 compares and contrasts specific aspects of the microstructure that are and are not resolved at the different scales. More detailed review on volume averaged methods is provided in Subsection 5.1, while review on the explicit microstructure prediction methods at the grain and sub-grain scale are provided in Subsections 5.2 and 5.3, respectively.

**Table 2. Microstructural details resolved by modeling at different scales**

	Morphology-scale	Grain-scale	Volume Averaged
As-solidified solute distribution profile around primary solidification structure	Yes	No	Partial
As-solidified primary solidification structure details (cells, branching of dendrites, bands)	Yes	No	Partial
As-solidified phases present	Yes	Partial	Partial
As-solidified texture	Partial	Yes	No
As-solidified grain size and shape distribution	Partial	Yes	Partial
Post-processing sub-grain phase and solute distribution	Yes	No	No
Post-processing grain size and shape distribution	Partial	Yes	No
Post-processing texture	Partial	Yes	No

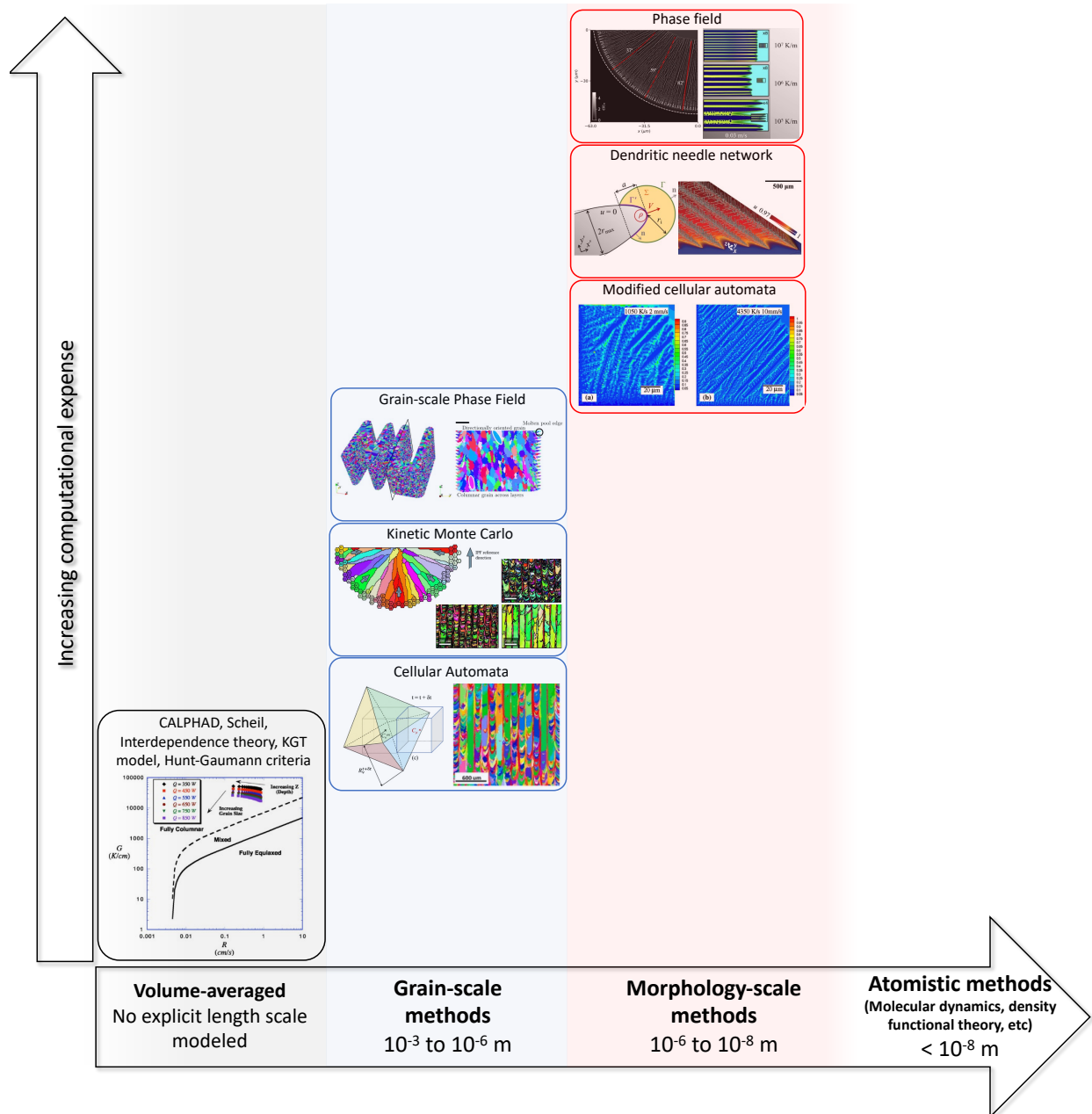


**Figure 6. Summary of the length scales for morphology-scale, grain-scale, and volume averaged solidification models, along with the level of complexity associated with the most commonly used modeling methods for each scale. Images adapted from [103, 104, 105, 106, 107, 108, 109, 110, 111].**

**5.1 VOLUME AVERAGED METHODS**

Perhaps the most common technique for understanding microstructural evolution is the so-called CALculation of PHase Diagrams, or CALPHAD [112]. This is a family of techniques used to describe the free energy of various phases under different conditions in order to calculate relative phase stability and

other subsequent quantities of interest. Accurate calculation requires semi-empirical calibration of the thermodynamic parameters describing each phase, which is usually done through incorporation of experimental observations for specific compositions and thermal conditions, or through first-principals simulations [113]. When used correctly, CALPHAD techniques are a powerful approach to understanding phase equilibria even for complex alloy systems, and a variety of commercial software packages and associated alloy databases are commercially available. These thermodynamic descriptions may be used to provide input to other models; examples of such input include phase diagram behavior for the analytical models or rules-driven morphological models described below, or free energy functions for phase field models. One example of the use of these techniques is Scheil calculations of solidification pathways, which assume complete mixing of solute in the liquid but no diffusion in the solid. These assumptions are reasonable for most faster solidification processes, including those found in AM. These types of solidification calculations can be useful for describing the phases expected in the as-solidified microstructure [114], propensity for solidification cracking [115, 116], or for describing the evolution of latent heat in the mushy zone during solidification of the melt pool [63]. CALPHAD may also be combined with databases for kinetics to estimate the nucleation, growth, size distributions, and strengthening effect of precipitates that form in the solid state [117].

Analytical methods consider the average or steady-state evolution of a given feature or features of the microstructure. These models do not output an explicit representation of a microstructure, instead using approximate mathematical relationships that govern the physics of interest and solving a series of equations for particular unknowns. Examples of this include the model of Kurz, Giovanola, and Trivedi (KGT), which approximates dendrite tip radius and velocity as functions of undercooling for an isolated dendrite tip solidifying in a domain with a positive thermal gradient and static, uniform cooling rate [118], as well as related models of primary dendrite arm spacing [119]. Additional relationships of feature size, velocity, and spacing to account for multicomponent [120] and multiphase solidification [121, 122, 123] have also been proposed. The transition from columnar grain structures to equiaxed grain structures (CET), commonly observed in casting microstructures though less so in AM, was modeled by [124] through calculation of a volume fraction of equiaxed grains as a function of alloy composition and thermal conditions during directional solidification. This analysis was later extended by [125] to use the KGT model for dendrite tip velocity as a function of undercooling.

Modeling efforts on the effect of phase diagram on promotion of the CET was summarized in a recent review article [126]. The interdependence model, developed by [127], relates grain size to the density and undercooling needed for activation of nucleant particles, solute partitioning, and solute diffusion coefficient. The growth restriction factor  $Q$  is associated with increased solutal undercooling ahead of the solidification front, and in turn, activation of nucleant particles and refinement of the as-solidified microstructure. The models of the CET allow process maps of “columnar”, “mixed”, and “equiaxed” grain structures to be constructed in thermal gradient ( $G$ ) - solidification velocity ( $V$ ) space, and as a function of alloy composition. As  $G$  and  $V$  are functions of the processing conditions during AM, maps of expected grain structure in process space (typically beam power and velocity) can be constructed [128, 129, 103]. More complex process maps that include both the solidification morphology and phase(s) present for a given set of  $G$  and  $V$  have also been constructed for laser processing [130].

The analytical models require minimal inputs and computational cost and can give a quick and often reasonable approximation of an average feature of an expected grain structure, such as the undercooling at which solidification occurs or the solidification morphology. However, the extreme conditions of AM will affect the accuracy of these relationships, many of which were developed for application to conditions

common to casting solidification. For example, the effect of  $Q$  in promoting the CET may be limited in AM melt pools due to the large  $G$  present, reducing the length of the constitutionally undercooled region ahead of the solidification front [131]. Models of the dendrite tip operating point such as the KGT model assume a steady state that may not be reached during the rapid solidification and relatively small (compared to casting) length scales of AM melt pools. The thermal gradient direction, in which cellular and dendritic solidification is favored, varies as a function of location in a given melt pool and in time, and the orientation of the substrate grains (from a baseplate or from previously deposited layers) introduces a scan path and melt pool shape dependence of grain size and shape that is not captured in process maps of the CET. As noted by [126], grain refinement during AM is heavily dependent on the density of nucleant particles and the size of said particles (related to the undercooling at which they are activated); these quantities are difficult to measure experimentally and will vary as a function of specific AM process and material. The accuracy of process maps is therefore tied to appropriate estimates for nucleation model inputs, which may not be available for all alloys or AM processing conditions.

## **5.2 EXPLICIT MICROSTRUCTURE MODELING METHODS: SUB-GRAIN SCALE**

Sub-grain scale (morphology-scale) models differ from analytical models in that they provide an explicit prediction of the microstructure rather than a purely mathematical one. These models predict the morphology of the solidification front (cellular, dendritic, banded, planar), the phase or phases present, the distribution of solute in the as-solidified material, and quantities such as the primary or secondary dendrite arm spacing. In turn, these models require additional information from heat transport models other than  $G$  and  $V$  at the solidification front; the full time-temperature history from a heat transport model is needed. Sub-grain scale models can either be strongly coupled to the heat transport model (two-way passing of information, where temperature is used by the solidification model to compute phase fractions that are used by the heat transport model) or weakly coupled (one-way passing of temperature information to the solidification model, and independent tracking of the solidification front by the heat transport model) [99]. While the evolution of latent heat is more accurately modeled using the strongly coupled approach, it is significantly more computationally expensive than the weakly coupled approach, which is more commonly used.

The phase field (PF) method is the most commonly used method to model the morphology of individual grains or regions of a microstructure. PF models solve equations for the evolution of order parameters that describe the system state to minimize the free energy of the system [132]. As noted by [133], this has the advantage of directly evolving a system towards thermodynamic equilibrium in real time. PF models have been applied to multiphase solidification, such as eutectic growth [134] and peritectic growth of ferrite and austenite phases in steel [135]. PF simulations have also successfully reproduced the microsegregation profile and primary dendrite arm spacing in 2D regions of AM melt pools [114, 136], orientation-dependent dendrite competition [110] and the columnar to equiaxed grain structure transition for a dendritic structure in 3D under representative AM conditions [137]. A series of 2D PF simulations using CALPHAD data and varying undercooling over a wide range was shown to compare favorably to the analytical KGT model predictions for large thermal gradient conditions, and the transition from dendritic and cellular to segregationless solidification morphology was predicted [107]. However, simulation at the thin interface limit is necessary for PF results to match experimental results [138], which in turn necessitates a sufficiently fine mesh to capture the curvature of dendrite tips. This creates a significant limitation on the size of the domain that can be simulated, particularly in 3D [99]. While recent GPU parallelization and the use of supercomputers has allowed accelerated PF calculations [139, 140], a recent

2D simulation on GPU with hundreds of dendrites was still reported to take 3.5 days to simulate 1 second of real time [141] (though notably this simulation included solid and liquid motion and solid coalescence, phenomena rarely or never accounted for in many other morphology-scale solidification methods). A large number of input parameters, many of which are temperature dependent and require prior atomistic or thermodynamic modeling data, are necessary for accurate PF simulation; however, it was noted in a recent review article that the large number of input parameters allows exact calibration of experimental results, which is not necessarily possible with other morphology-scale approaches [98].

Cellular automata (CA, often called a modified CA to distinguish it from the CA-based grain scale approach) methods can also be applied to the simulation of grain morphology [142]. Unlike the PF approach, the modified CA has a sharp interface at which solute partitioning and curvature are calculated and used to update the simulation using rules based on phase diagram approximations and interfacial energy [143]. This approach has commonly been applied to thermal conditions often encountered in casting processes to predict dendrite arm spacing [144], the effect of fluid flow on dendritic solidification [145, 146], and both columnar and equiaxed growth [147], though some recent papers have applied it to the more extreme conditions encountered in subsections of AM melt pools [104, 148]. The simplistic nature of the modified CA method makes it less computationally expensive than PF simulations [97] and able to reproduce PF results under certain conditions [149]. However, the rules-based nature of the method can render it prone to grid dependence and limited to qualitative reproduction of experimentally observed solidification morphologies. Additionally, as a fine cell size is still required to accurately resolve the curvature at the dendrite tips, the method is still relatively computationally intensive.

Additional methods have attempted to bridge the divide between the more physically-based PF and more computationally-tractable modified CA approach. The dendritic needle network (DNN) method tracks individual branches of dendrites using velocities and radii calculated using relationships from solidification theory and a reduced form of the solute field [150, 151]. The resulting microsegregation pattern from DNN simulations compares favorably to those predicted by PF [106] and has been validated against directional solidification experiments and successfully modeled the CET [105, 152]. Additionally, a DNN-inspired model has been used to model epitaxial solidification in AM melt pools [153]. DNN simulations have also been coupled with fluid flow to show the effect on the primary arm spacing and side branching [154]. Hybrid models combining components of Phase Field and Cellular Automata to balance the thermodynamic basis of the former and the efficiency of the latter have also been implemented [155, 156, 157] and in some cases applied to AM problems [156]. However, these intermediate scale approaches have not been commonly used for simulation of AM solidification problems.

### **5.3 EXPLICIT MICROSTRUCTURE MODELING METHODS: GRAIN SCALE**

Explicit simulation of the microstructure can also be performed at the coarser length scale of the grains themselves. While grain-scale approaches do not explicitly predict the details of solute segregation patterns within the grain nor the solute transport surrounding the grains, approximations regarding the sub-grain scale behavior allow prediction of larger regions of microstructure with a significantly reduced computational cost. A grain-scale form of the phase field method can be applied to this problem, where order parameters represent grain ID and orientation, and free energy evolution includes the effects of grain boundary orientation and grain orientation relative to the thermal gradient direction. The grain scale PF model has been applied to AM problems, simulating coupled nucleation and solidification with a temperature-dependent rate coefficient and solid-solid grain boundary motion [158]. It has also simulated phenomena such as texture development, powder particle sintering, and powder consolidation for

calculations of porosity and grain size [153, 126]. While this approach is more flexible than the rules-based approaches described next, it remains significantly more computationally intensive (though promising efforts using graph theory have been made to accelerate these calculations [111]) and has thus far been limited to 2D subsections of AM melt pools or small 3D sections.

Cellular automata (CA) methods have been the most commonly-used simulation tool for grain-scale microstructure development modeling. Unlike grain-scale PF, which can simulate transient grain evolution, CA is limited to a quasi-steady state approximation of interfacial advance as a function of local undercooling. It also typically assumes the dendritic solidification mode, using octahedron-based tracking of the solidification front to approximate the preferential  $\langle 100 \rangle$  crystal growth directions in BCC and FCC alloys [159]. As CA reduces the solidification problem to relatively simple algebraic and geometric relationships, it is computationally efficient and has been applied extensively to simulate grain size distribution and texture development first for casting problems, and more recently for AM problems. Simulated grain structures consisting of many layers in 3D have shown agreement with experimental results for laser AM processing of stainless steel 304 [160], stainless steel 316L [161, 162], AISi10Mg [163], AA-2024 [164], Inconel 718 [165, 166, 167], and electron beam AM processing of Inconel 718 [168], Ti-6Al-4V [166] and CMSX-4 Ni superalloy [169]. Typically, the limiting factor in CA model performance is the generation of the temperature field data, as many CA models are at least one-way if not two-way coupled to a heat transport solver. Notably, the ExaCA code avoids this limitation by using a sparse form of the time-temperature history data from an external heat transport model as input, using this data to model large AM microstructures on GPU in a matter of hours [170].

Kinetic Monte Carlo (kMC) models are similar to CA in that they have discrete lattice spacing and state variables for grain orientations. Unlike CA models, which are based on algebraic or geometrical approximations of the solidification front movement, kMC models use probability-based evolution rules for grain states. Probabilities are related to the energy change of the system; system changes that reduce the energy of the system are always accepted, and others have only a calculated probability of being accepted. Like CA, kMC was originally applied to casting problems and has recently been applied to AM. Liquid-solid and solid-solid phase transformation during AM processing has been simulated with kMC and successfully predicted multiple aspects of grain AM structures for Ni superalloys, titanium alloys, and steel [171, 108, 172, 133]. However, accurately modeling texture using kMC necessitates that the probabilities allow preferential advance of grains with orientations near the local thermal gradient direction at a given point in time; while tuning of these probabilities may provide the ability to calibrate kMC models to experimental results better than CA (though without a true physical basis), calculation of the interface orientation and probabilities for each lattice point on the interface each time step can be computationally expensive. It was noted by [173] that CA was more efficient than kMC in the modeling of an equiaxed microstructure as CA does not require probability calculation allowing larger time steps, but no study comparing the efficiency of the two methods for AM problems has been performed to date.

## **6. RECOMMENDATIONS FOR PROCESS MODELING DEVELOPMENTS FOR PREDICTING AM VARIABILITY**

Based on the above review, there are a variety of potential developments which would increase the ability of process modeling tools to explain variability of microstructure and properties of AM builds using SS316 alloys. Some of these advances involve the use of existing models, others require significant improvements relative to the current state-of-the-art, and still others are based around the industrial environment and practical application of these tools. A key consideration when evaluating these advances is being able to achieve a combination of model prediction accuracy and computational efficiency that is suitable for considering component-scale effects and for regular industrial use on modest computing systems. Below, we describe several of these advances with the specific goal of capturing component scale variability.

### **6.1 MODELING AND METHODOLOGY IMPROVEMENTS**

Thermomechanical models are capable of reasonably predicting part-scale residual stress distributions; however, fully coupled models are computationally intensive, while simplified inherent strain based models require careful calibration, and may not translate accurately between process conditions and geometries. Assuming that near-term application of these models will favor the inherent strain technique due to its computational efficiency, additional research is necessary to automate the calibration process and to support it with experimental data. Ideally, experimental trials that measure residual stress distributions over a wide range of processing conditions and geometries would be used as a benchmark for simulation results. Additionally, analysis of the simulations could help to understand the sensitivity of the calibrations to particular parameters, and assess whether a model is or is not valid in a given situation. This calibration and analysis may be an opportunity for the application of AI/ML techniques.

Melt pool models perhaps cover the widest range of formulations and associated computational expense. The most sophisticated models that include details of fluid flow and free surface deformation are too computationally intensive for use in anything but a targeted scientific context. Furthermore, the significant uncertainty in surface tension gradients as a function of temperature create challenges in prediction of fluid mechanics. As a result, conduction-based models are attractive for near term application as they balance computational expense and physical fidelity. However, additional research is necessary to improve the predictive capabilities of these models by designing reasonable effective heat sources to account for effects such as fluid mechanics and keyhole formation. There is a risk in this approach of calibrating models too narrowly by prescribing heat source shapes that are only suitable for a specific set of local conditions; therefore, development of physics-driven effective heat sources that naturally account for sub-scale phenomena in a reasonable way is of significant interest. Additionally, well assessed techniques for calibration will be necessary, both in terms of experimental design as well as computational approaches for incorporating experimental data and assessing the range of applicability of a given calibration.

There are also significant opportunities for semi-analytical modeling. The major disadvantage of these approaches is the limited selection of heat source geometries and simplifications to the boundary conditions at the interface between the component and the powder bed. For these reasons, the model results are probably not suitable for passing melt pool data models that are very sensitive to melt pool shape, for example, sub-scale microstructure models. However, semi-analytical models provide a rapid method to assess general trends in melt pool behavior in response to complex scan patterns. These tools could be a useful first approximation of thermal conditions for use in focusing the application of more complex models, or for integration with a larger workflow (see subsection below).

In microstructure modeling, the relevant length and time scale are necessarily very small compared to those of the component scale. Of the various modeling approaches, only analytical forms for estimating microstructure evolution are suitable for application across longer scales. Analytical models for estimating microstructure behavior could be coupled with melt pool models to predict distributions of features such as dendrite arm spacing. There are also opportunities to utilize thermo-kinetic modeling to predict quantities such as microsegregation, phase selection, or in situ precipitation.

Many quantities of interest, such as details of grain or precipitate structure, cannot be reasonably predicted without an explicit description of the microstructure. In this case, CA models appear to be the best compromise between predicting physically meaningful quantities (e.g., grain size, aspect ratio, and texture) with reasonable computational expense, but have inherent challenges with parallelization. CA can currently be applied to representative volume elements (e.g., a 1 mm cube) but rarely, if ever, on larger scales that might capture spatial variability in component performance. New solution techniques may be able to improve performance and scalability, making this type of modeling more accessible for a broader range of processing conditions and materials systems. Collecting meaningful calibration and validation data is a significant challenge since grain structures in AM components are frequently complex and challenging to perfectly represent statistically. Three-dimensional experimental data sets could be extremely valuable for comparison to computational predictions, but are currently expensive and challenging to collect and analyze.

More expensive microstructural models, such as phase field simulations, are unlikely to be directly applicable to understanding process variability in the near-term. However, they may have an indirect impact in helping to parameterize more efficient simplified models or helping to direct the study of the variations in thermal conditions. For example, the dendrite growth kinetics observed in phase field models may be used to more accurately estimate the interface response function describing the relationship between undercooling and dendrite growth velocity within CA models. Dendrite resolved models (phase field, microscale CA, or DNN) can also predict features such as secondary arm branching, and phase field in particular can reproduce transitions between planar, cellular, and dendritic growth. These types of capabilities may inform further both the development and application of models at larger length scales. A major limitation now is that these models, phase field in particular, tend to simplify the composition effects of complex alloys down to representative binary or ternary systems. For relevance to commercial alloys that frequently include many more alloying additions, more complex consideration of the thermodynamics and solute fields will be necessary.

## **6.2 WORKFLOW OPPORTUNITIES**

While example workflows for coupling simulation of the thermal conditions and with either simulated microstructure or simulated residual stress calculations exist, those workflows have largely been used for scientific applications; moreover, those workflows generally focus simulation efforts on a small volume of an entire part and generally require the use of high performance computing clusters to achieve tractable computation times. In order to leverage these workflows for understanding process variability at the component scale, either the computational cost of the models in the workflow needs to be reduced or a new approach needs to be developed which bridges the length-scale gap between the melt pool and the component. It is likely that a path forward will involve both a reduction in computational cost and a new approach to bridging the melt pool and component scales. Additionally, since the development costs of new models and workflows needs to be considered as a barrier to creating convenient, automated workflows, new workflows will likely consist of a collection of models developed by researchers from

different groups and institutions; however, creating automated communication of inputs and outputs between different models has been demonstrated to be a complex task.

Given the computational expense of models that are of significant interest to accurately describing the melt pool behavior and microstructure evolution, a potential approach is to focus on accurate simulation of carefully selected representative volume elements (RVEs). The simulation of select RVEs presents its own challenges for developing a usable, and preferably automated, workflow. First, the coupling between models, specifically between melt pool and microstructure simulations, needs to be carefully considered. The melt pool model must be capable of capturing longer length scale heat transfer effects across the component geometry, although areas far from a selected RVE do not necessarily require resolutions at the melt pool scale. Within a selected RVE, the melt pool dynamics need to be carefully calibrated and validated, and the data on the resulting solidification conditions needs to be communicated to the microstructural length scale with minimum overhead for storing and transferring data. The size of the RVE also needs to be determined such that relevant statistics of the microstructure (e.g., texture) may be accurately determined and edge effects from the domain boundary may be reasonably neglected.

Assuming the model coupling within a given RVE is adequate, a second consideration is the selection of RVEs given geometry and scan path information. For this purpose, identifying the distribution of thermal conditions across a component is important, and might be accomplished through use of semi-analytical melt pool models, or the lumped-layer approach implemented in coarse-grained thermomechanical simulations. It will be necessary to quantify the variation across components and to select localized regions that may act as RVEs using coupled higher fidelity simulations. The selection of RVEs given data from lower-fidelity models requires expert knowledge of the problem and application; however, AI/ML techniques may become a useful way to automate this selection process when given a large enough data set. Once the high-fidelity data has been computed for the RVEs, the data must be generalized back to the component scale. For this purpose, there is likely a role for data-driven, surrogate models, or AI/ML techniques which allow for interpolating the outputs from a handful of RVEs back to the entire domain based on the similarity between lower-fidelity thermal conditions observed within regions of the domain the lower-fidelity thermal conditions observed within the RVEs.

### **6.3 INDUSTRIAL ENVIRONMENT AND DATA INTEGRATION**

Aside from developments on the process modeling tools themselves, regular use of these tools requires certain aspects of the industrial environment within which they will be implemented. First, a requirement for all of the suggested modeling approaches is that the AM process itself is reasonably represented for a given combination of geometry, process conditions, and scan parameters. This includes detailed descriptions of the laser power, velocity, and trajectory over time. Unfortunately, this information is not always available. Some LPBF systems have open-source control systems that make it possible to design or extract scan path data, but tend to be designed as research tools and are not commonly used for industrial applications. Ideally, a next-generation of AM systems will be designed with opportunities for qualification and certification in mind. Given that the material microstructure and properties are inherently linked to these process conditions, it will be necessary to expose these details to understand the extent of variability within finished components.

A recurring theme within this report is the trade-off in model fidelity and computational expense. Development and selection of models to understand process variability will necessarily need to be fit to the available computational resources. Frequently, for industrial application, this may be limited to modest

computing clusters or workstations. This environment will certainly challenge the application of models that are designed to accurately resolve detailed information at a microstructural level. However, computational resources evolve quickly. Currently, emerging trends in cloud computing and edge computing resources may make more expensive models increasingly tractable in the near future. Industrial entities that wish to implement these tools should consider implementation of edge computing nodes corresponding to individual or small collections of AM systems. Simultaneously, developers of these simulation tools should make considerations for deployment on cloud computing systems.

Finally, the nature of the AM process lends itself to a data-rich environment. That is, process monitoring is frequently implemented to provide data on at least a layer-by-layer basis, if not more frequently, which may then be reconstructed to inform the three-dimensional status of the final component [33, 34]. In this sense, simulation data may act as an additional data stream meant to correspond with and complement observable process data. Together, the combination of data streams is likely to be more informative than individual data stream on its own. For example, in-process monitoring is increasingly used to identify defects within builds. In many cases, these types of defects are not explicitly considered in any type of modeling (e.g., recoater blade damage). On the other hand, modeling tools regularly predict quantities that are challenging or impossible to observe experimentally in real time. For example, the grain structure development during processing is dependent upon sub-surface melt pool dynamics not readily accessible to sensors such as optical pyrometers or infrared thermography. Given that the properties of the final material is anticipated to be strongly dependent on both microstructure and defect distributions, these data streams could conceivably be leveraged together to create a more complete picture of the process and resulting material quality.

A data-rich environment suggests opportunities for application of AI/ML techniques. These may take many forms in terms of automatically detecting processing defects, or even estimating material properties. They also suggest some additional requirements for process modeling tools if this data is to be incorporated into that data-driven workflow. The type and amount of data to be collected and stored must be carefully considered. Models using the small length scales necessary to capture microstructure produce enough data to quickly pose significant data storage challenges if put into regular use. As a result, lossy data compression techniques, such as storing a statistical representation of the data, become necessary; however, determining the appropriate quantities of interest to extract from full-featured data sets is a non-trivial challenge. The selected features should be light-weight, where possible, and also capture key physical elements of the material under consideration. Over time, collection of this data may lend itself to analysis using AI/ML tools which circumvents explicit modeling altogether by building a data-driven surrogate model for direct estimation of the statistical quantities of interest.

## 7. CONCLUSIONS

This report summarizes the general requirements and current status of process modeling tools that might be used to predict variability for SS316 components processed by laser powder bed fusion additive manufacturing. These tools consist of models for several types of physical effects: (1) residual stress and distortion; (2) melt pool dynamics; and (3) microstructure evolution. A major theme that emerged in the review of the current state-of-the-art of these models is the trade-off between the fidelity of the included physics in each case, and the computational expense of the resulting simulations. Predicting variability in AM processes requires an understanding of the location-to-location differences in thermal conditions and the resulting microstructure evolution. A major limitation of existing AM process models is their limited applicability to component-level length and time scales. As a result, there is need for both developments in the accuracy and efficiency of each type of model and also for an overall workflow that intelligently couples these models together to maximize the value of the data produced. This approach might be realized, for example, by utilizing lower-fidelity models that capture the minimum level of physics to select the conditions for which higher fidelity models may be run for specific sub-domains. Additionally, the data produced by the models and their incorporation with complementary experimental data was identified as a significant opportunity for the application of artificial intelligence and machine learning techniques.

An additional observation from the review of the literature is that development on process modeling has been understandably driven by the additive manufacturing research community. Consequently, general understanding of AM process dynamics has been a priority, often without specific applications in mind. This community driven approach has been extremely effective for rapidly maturing specific simulation techniques. However, industry specific challenges are likely to arise that are not currently considered. With nuclear energy applications in mind, there are particular performance and property metrics (such as radiation damage, swelling, etc.) with particular microstructural and processing considerations that may not be broadly applicable to other industries. As a result, those particular issues have not received meaningful attention from the community that is focused more generally on AM process modeling. The same situation is undoubtedly also true for other industries with specific and narrowly focused performance requirements. As these modeling tools continue to mature, it will be necessary for specific industries to guide development where necessary for the appropriate applications. For this purpose, the nuclear energy industry should consider a coordinated effort to identify the key microstructural and processing characteristics that are critical for key target application areas, with consideration, for example, for typical radiation effects that are unique to this industry. Proper identification of these linkages will help guide the development of models across the range of process-microstructure-property relationships to maximize the impact on accelerating adoption of AM.

## 8. REFERENCES

- [1] Meimei Li, David Andersson, Ryan Dehoff, Andrea Jokisaari, Isabella Van Rooyen, and Dirk Cairns-Gallimore. Department of Energy Office of Nuclear Energy Advanced Materials and Manufacturing Technologies (AMMT) 2022 Roadmap. Report ANL-23/12, 2022.
- [2] Narendran Raghavan, Benjamin C Stump, Patxi Fernandez-Zelaia, Michael M Kirka, and Srdjan Simunovic. Influence of geometry on columnar to equiaxed transition during electron beam powder bed fusion of IN718. *Additive Manufacturing*, 47:102209, 2021.
- [3] A. A. Antonysamy, J. Meyer, and P. B. Prangnell. Effect of build geometry on the  $\beta$ -grain structure and texture in additive manufacture of ti6al4v by selective electron beam melting. *Materials Characterization*, 84:153–168, 2013.
- [4] H. L. Wei, T. Mukherjee, W. Zhang, J. S. Zuback, G. L. Knapp, A. De, and T. DebRoy. Mechanistic models for additive manufacturing of metallic components. *Progress in Materials Science*, 116:100703, 2021.
- [5] A Plotkowski, J Ferguson, B Stump, W Halsey, V Paquit, C Joslin, SS Babu, A Marquez Rossy, MM Kirka, and RR Dehoff. A stochastic scan strategy for grain structure control in complex geometries using electron beam powder bed fusion. *Additive Manufacturing*, 46:102092, 2021.
- [6] R. R. Dehoff, M. M. Kirka, F. A. List, K. A. Unocic, and W. J. Sames. Crystallographic texture engineering through novel melt strategies via electron beam melting: Inconel 718. *Materials Science and Technology*, 31(8):939–944, 2015.
- [7] Tarasankar Debroy, Wei Zhang, J Turner, and Sudarsanam Suresh Babu. Building digital twins of 3d printing machines. *Scripta Materialia*, 135:119–124, 2017.
- [8] Werner Kritzing, Matthias Karner, Georg Traar, Jan Henjes, and Wilfried Sihn. Digital twin in manufacturing: A categorical literature review and classification. *IFAC-PapersOnLine*, 51(11):1016–1022, 2018.
- [9] T. DebRoy, H. L. Wei, J. S. Zuback, T. Mukherjee, J. W. Elmer, J. O. Milewski, A. M. Beese, A. Wilson-Heid, A. De, and W. Zhang. Additive manufacturing of metallic components—process, structure and properties. *Progress in Materials Science*, 150:304–313, 2018.
- [10] K. L. Murty and I. Charit. Structural materials for gen-iv nuclear reactors: Challenges and opportunities. *Journal of Nuclear Materials*, 383(1):189–195, 2008.
- [11] William R Corwin. Us generation iv reactor integrated materials technology program. *Nuclear engineering and technology*, 38(7):591–618, 2006.
- [12] H. Schroeder. High temperature embrittlement of metals by helium. *Radiation Effects*, 78(1-4):297–314, 1983.
- [13] R. L. Klueh. Elevated temperature ferritic and martensitic steels and their application to future nuclear reactors. *International Materials Reviews*, 50(5):287–310, 2005.
- [14] Amy J. Godfrey, J. Simpson, D. Leonard, K. Sisco, R. R. Dehoff, and S. S. Babu. Heterogeneity and solidification pathways in additively manufactured 316L stainless steels. *Metallurgical and Materials Transactions A*, 2022.

- [15] Kee Bong Yoon, Van Hung Dao, and Jong Min Yu. Effects of build direction on tensile and creep properties of 316L stainless steel produced by selective laser melting. *Fatigue & Fracture of Engineering Materials & Structures*, 43(11):2623–2636, 2020.
- [16] Ronald Lesley Plaut, Clara Herrera, Doris Maribel Escriba, Paulo Rangel Rios, and Angelo Fernando Padilha. A short review on wrought austenitic stainless steels at high temperatures: processing, microstructure, properties and performance. *Materials Research*, 10:453–460, 2007.
- [17] Shao-Pu Tsai, Surendra Kumar Makineni, Baptiste Gault, Kaori Kawano-Miyata, Akira Taniyama, and Stefan Zaeferrer. Precipitation formation on  $\Sigma 5$  and  $\Sigma 7$  grain boundaries in 316L stainless steel and their roles on intergranular corrosion. *Acta Materialia*, 210:116822, 2021.
- [18] Kirstin Riener, Nikolaj Albrecht, Stefan Ziegelmeier, Robert Ramakrishnan, Lukas Haferkamp, Adriaan B. Spierings, and Gerhard J. Leichtfried. Influence of particle size distribution and morphology on the properties of the powder feedstock as well as of AlSi10Mg parts produced by laser powder bed fusion (LPBF). *Additive Manufacturing*, page 101286, 2020.
- [19] Cang Zhao, Bo Shi, Shuailei Chen, Dong Du, Tao Sun, Brian J. Simonds, Kamel Fezzaa, and Anthony D. Rollett. Laser melting modes in metal powder bed fusion additive manufacturing. *Reviews of Modern Physics*, 94(4):045002, 2022.
- [20] Hiroki Amano, Takuya Ishimoto, Koji Hagihara, Ryoya Suganuma, Keisuke Aiba, Shi-Hai Sun, Pan Wang, and Takayoshi Nakano. Impact of gas flow direction on the crystallographic texture evolution in laser beam powder bed fusion. *Virtual and Physical Prototyping*, 18(1):e2169172, 2023.
- [21] Jithin James Marattukalam, Dennis Karlsson, Victor Pacheco, Přemysl Beran, Urban Wiklund, Ulf Jansson, Björgvin Hjörvarsson, and Martin Sahlberg. The effect of laser scanning strategies on texture, mechanical properties, and site-specific grain orientation in selective laser melted 316L SS. *Materials & Design*, 193:108852, 2020.
- [22] O. Zinovieva, V. Romanova, and R. Balokhonov. Effects of scanning pattern on the grain structure and elastic properties of additively manufactured 316L austenitic stainless steel. *Materials Science and Engineering: A*, 832:142447, 2022.
- [23] M. C. Brennan, J. S. Keist, and T. A. Palmer. Defects in metal additive manufacturing processes. *Journal of Materials Engineering and Performance*, 30:4808–4818, 2021.
- [24] Luqing Cui, Shuang Jiang, Jinghao Xu, Ru Lin Peng, Reza Taherzadeh Mousavian, and Johan Moverare. Revealing relationships between microstructure and hardening nature of additively manufactured 316L stainless steel. *Materials & Design*, 198:109385, 2021.
- [25] Matthias Markl and Carolin Körner. Multiscale modeling of powder bed-based additive manufacturing. *Annual Review of Materials Research*, 46(1):93–123, 2016.
- [26] W. King, A. T. Anderson, R. M. Ferencz, N. E. Hodge, C. Kamath, and S. A. Khairallah. Overview of modelling and simulation of metal powder bed fusion process at Lawrence Livermore National Laboratory. *Materials Science and Technology*, 31(8):957–968, 2015.
- [27] Mohamad Bayat, Wen Dong, Jesper Thorborg, Albert C. To, and Jesper H. Hattel. A review of multi-scale and multi-physics simulations of metal additive manufacturing processes with focus on modeling strategies. *Additive Manufacturing*, 47:102278, 2021.

- [28] John A Turner, James Belak, Nathan Barton, Matthew Bement, Neil Carlson, Robert Carson, Stephen DeWitt, Jean-Luc Fattebert, Neil Hodge, Zechariah Jibben, Wayne King, Lyle Levine, Christopher Newman, Alex Plotkowski, Balasubramaniam Radhakrishnan, Samuel Temple Reeve, Matthew Rolchigo, Adrian Sabau, Stuart Slattery, and Benjamin Stump. ExaAM: Metal additive manufacturing simulation at the fidelity of the microstructure. *The International Journal of High Performance Computing Applications*, 36(1):13–39, 2022.
- [29] C. Bierwisch, A. Butz, B. Dietemann, A. Wessel, T. Najuch, and S. Mohseni-Mofidi. PBF-LB/M multiphysics process simulation from powder to mechanical properties. *Procedia CIRP*, 111:37–40, 2022.
- [30] Lyle Levine, Brandon Lane, Jarred Heigel, Kalman Migler, Mark Stoudt, Thien Phan, Richard Ricker, Maria Strantza, Michael Hill, Fan Zhang, Jonathan Seppala, Edward Garboczi, Erich Bain, Daniel Cole, Andrew Allen, Jason Fox, and Carelyn Campbell. Outcomes and conclusions from the 2018 AM-Bench measurements, challenge problems, modeling submissions, and conference. *Integrating Materials and Manufacturing Innovation*, 9(1):1–15, 2020.
- [31] America Makes & ANSI Additive Manufacturing Standardization Collaborative. Standardization roadmap for additive manufacturing: Version 2. Report, ANSI and NDCMM/America Makes, 2018.
- [32] Matthew Rolchigo, Benjamin Stump, James Belak, and Alex Plotkowski. Sparse thermal data for cellular automata modeling of grain structure in additive manufacturing. *Modelling and Simulation in Materials Science and Engineering*, 28(6):065003, 2020.
- [33] Luke Scime, Derek Siddel, Seth Baird, and Vincent Paquit. Layer-wise anomaly detection and classification for powder bed additive manufacturing processes: A machine-agnostic algorithm for real-time pixel-wise semantic segmentation. *Additive Manufacturing*, 36:101453, 2020.
- [34] Luke Scime, Alka Singh, and Vincent Paquit. A scalable digital platform for the use of digital twins in additive manufacturing. *Manufacturing Letters*, 31:28–32, 2022.
- [35] Mojtaba Mozaffar, Shuheng Liao, Xiaoyu Xie, Sourav Saha, Chanwook Park, Jian Cao, Wing Kam Liu, and Zhengtao Gan. Mechanistic artificial intelligence (Mechanistic-AI) for modeling, design, and control of advanced manufacturing processes: Current state and perspectives. *Journal of Materials Processing Technology*, page 117485, 2021.
- [36] Xiaoyu Xie, Jennifer Bennett, Sourav Saha, Ye Lu, Jian Cao, Wing Kam Liu, and Zhengtao Gan. Mechanistic data-driven prediction of as-built mechanical properties in metal additive manufacturing. *npj Computational Materials*, 7(1):86, 2021.
- [37] Y. Du, T. Mukherjee, and T. DebRoy. Physics-informed machine learning and mechanistic modeling of additive manufacturing to reduce defects. *Applied Materials Today*, 24:101123, 2021.
- [38] Lameck Mugwagwa, Ina Yadroitsava, Nkutowane Washington Makoana, and Igor Yadroitsev. Residual stress in laser powder bed fusion. In *Fundamentals of Laser Powder Bed Fusion of Metals*, pages 245–276. Elsevier, 2021.
- [39] P.J. Withers and H.K.D.H. Bhadeshia. Residual stress. Part 1 – measurement techniques. *Materials Science and Technology*, 17(4):355–365, 2001.

- [40] G.A. Webster and A.N. Ezeilo. Residual stress distributions and their influence on fatigue lifetimes. *International Journal of Fatigue*, 23:375–383, 2001.
- [41] G Vanboven, W Chen, and R Rogge. The role of residual stress in neutral pH stress corrosion cracking of pipeline steels. Part I: Pitting and cracking occurrence. *Acta Materialia*, 55(1):29–42, 2007.
- [42] Mustafa Megahed, Hans-Wilfried Mindt, Narcisse N’Dri, Hongzhi Duan, and Olivier Desmaison. Metal additive-manufacturing process and residual stress modeling. *Integrating Materials and Manufacturing Innovation*, 5:61–93, 2016.
- [43] Lars-Erik Lindgren and Andreas Lundbäck. Approaches in computational welding mechanics applied to additive manufacturing: Review and outlook. *Comptes Rendus Mécanique*, 346(11):1033–1042, 2018.
- [44] Ze-Chen Fang, Zhi-Lin Wu, Chen-Guang Huang, and Chen-Wu Wu. Review on residual stress in selective laser melting additive manufacturing of alloy parts. *Optics & Laser Technology*, 129:106283, 2020.
- [45] Patcharapit Promoppatum and Vitoon Uthaisangsuk. Part scale estimation of residual stress development in laser powder bed fusion additive manufacturing of Inconel 718. *Finite Elements in Analysis and Design*, 189:103528, 2021.
- [46] P Prabhakar, William J Sames, R Dehoff, and Sudarsanam Suresh Babu. Computational modeling of residual stress formation during the electron beam melting process for Inconel 718. *Additive Manufacturing*, 7:83–91, 2015.
- [47] RK Ganeriwala, Maria Strantza, WE King, Bjorn Clausen, Thien Q Phan, Lyle E Levine, Donald W Brown, and NE Hodge. Evaluation of a thermomechanical model for prediction of residual stress during laser powder bed fusion of Ti-6Al-4V. *Additive Manufacturing*, 27:489–502, 2019.
- [48] J Goldak, J Zhou, V Breiguine, and F Montoya. Thermal stress analysis of welds: from melting point to room temperature. *Transactions of JWRI*, 25(2):185–189, 1996.
- [49] Rishi K Ganeriwala, Neil E Hodge, and Jerome M Solberg. Towards improved speed and accuracy of laser powder bed fusion simulations via multiscale spatial representations. *Computational Materials Science*, 187:110112, 2021.
- [50] Yukio Ueda, Keiji Fukuda, Keiji Nakacho, and Setsuo Endo. A new measuring method of residual stresses with the aid of finite element method and reliability of estimated values. *Journal of the Society of Naval Architects of Japan*, 1975(138):499–507, 1975.
- [51] Nils Keller and Vasily Ploshikhin. New method for fast predictions on residual stress and distortion of AM parts. In *2014 International Solid Freeform Fabrication Symposium*. University of Texas at Austin, 2014.
- [52] Qian Chen, Xuan Liang, Devlin Hayduke, Jikai Liu, Lin Cheng, Jason Oskin, Ryan Whitmore, and Albert C To. An inherent strain based multiscale modeling framework for simulating part-scale residual deformation for direct metal laser sintering. *Additive Manufacturing*, 28:406–418, 2019.
- [53] Xuan Liang, Qian Chen, Lin Cheng, Qingcheng Yang, and Albert To. A modified inherent strain

- method for fast prediction of residual deformation in additive manufacturing of metal parts. In *2017 International Solid Freeform Fabrication Symposium*. University of Texas at Austin, 2017.
- [54] Yanfei Wang, Quan Li, Lingyun Qian, and Yabin Yang. A modified inherent strain model with consideration of the variance of mechanical properties in metal additive manufacturing. *Journal of Manufacturing Processes*, 72:115–125, 2021.
- [55] Hossein Mohammadtaheri, Ramin Sedaghati, and Marjan Molavi-Zarandi. Inherent strain approach to estimate residual stress and deformation in the laser powder bed fusion process for metal additive manufacturing—a state-of-the-art review. *The International Journal of Advanced Manufacturing Technology*, 122(5-6):2187–2202, 2022.
- [56] Nachiket Patil, Rishi Ganeriwala, Jerome M Solberg, Neil E Hodge, and Robert M Ferencz. Benchmark multi-layer simulations for residual stresses and deformation in small additively manufactured metal parts. *Additive Manufacturing*, 45:102015, 2021.
- [57] Matteo Bugatti and Quirico Semeraro. Limitations of the inherent strain method in simulating powder bed fusion processes. *Additive Manufacturing*, 23:329–346, 2018.
- [58] Iñaki Setien, Michele Chiumenti, Sjoerd van der Veen, Maria San Sebastian, Fermín Garcíandía, and Alberto Echeverría. Empirical methodology to determine inherent strains in additive manufacturing. *Computers & Mathematics with Applications*, 78(7):2282–2295, 2019.
- [59] Lun Li and Sam Anand. Hatch pattern based inherent strain prediction using neural networks for powder bed fusion additive manufacturing. *Journal of Manufacturing Processes*, 56:1344–1352, 2020.
- [60] Ross Cunningham, Cang Zhao, Niranjana Parab, Christopher Kantzos, Joseph Pauza, Kamel Fezzaa, Tao Sun, and Anthony D. Rollett. Keyhole threshold and morphology in laser melting revealed by ultrahigh-speed x-ray imaging. *Science*, 363(6429):849–852, 2019.
- [61] Jordan S. Weaver, Jarred C. Heigel, and Brandon M. Lane. Laser spot size and scaling laws for laser beam additive manufacturing. *Journal of Manufacturing Processes*, 73:26–39, 2022.
- [62] Benjamin Stump and Alex Plotkowski. An adaptive integration scheme for heat conduction in additive manufacturing. *Applied Mathematical Modelling*, 75:787–805, 2019.
- [63] J. Coleman, A. Plotkowski, B. Stump, N. Raghavan, A. S. Sabau, M. J. M. Krane, J. Heigel, R. E. Ricker, L. Levine, and S. S. Babu. Sensitivity of thermal predictions to uncertain surface tension data in laser additive manufacturing. *Journal of Heat Transfer*, 142(12):122201, 2020.
- [64] Saad A Khairallah, Andrew T Anderson, Alexander Rubenchik, and Wayne E King. Laser powder-bed fusion additive manufacturing: Physics of complex melt flow and formation mechanisms of pores, spatter, and denudation zones. *Acta Materialia*, 108:36–45, 2016.
- [65] Daniel Rosenthal. The theory of moving sources of heat and its application to metal treatments. *Transactions of the American Society of Mechanical Engineers*, 68(8):849–865, 1946.
- [66] Ming Tang, P Chris Pistorius, and Jack L Beuth. Prediction of lack-of-fusion porosity for powder bed fusion. *Additive Manufacturing*, 14:39–48, 2017.

- [67] Jian Liu and Albert C To. Quantitative texture prediction of epitaxial columnar grains in additive manufacturing using selective laser melting. *Additive Manufacturing*, 16:58–64, 2017.
- [68] TW Eagar, NS Tsai, et al. Temperature fields produced by traveling distributed heat sources. *Welding journal*, 62(12):346–355, 1983.
- [69] NT Nguyen, A Ohta, K Matsuoka, N Suzuki, and Y Maeda. Analytical solutions for transient temperature of semi-infinite body subjected to 3-D moving heat sources. *Welding Journal*, 78:265–s, 1999.
- [70] Robert Forslund, Anders Snis, and Stig Larsson. Analytical solution for heat conduction due to a moving gaussian heat flux with piecewise constant parameters. *Applied Mathematical Modelling*, 66:227–240, 2019.
- [71] Edwin J Schwalbach, Sean P Donegan, Michael G Chapman, Kevin J Chaput, and Michael A Groeber. A discrete source model of powder bed fusion additive manufacturing thermal history. *Additive Manufacturing*, 25:485–498, 2019.
- [72] Benjamin Stump and Alex Plotkowski. Spatiotemporal parallelization of an analytical heat conduction model for additive manufacturing via a hybrid OpenMP+ MPI approach. *Computational Materials Science*, 184:109861, 2020.
- [73] Sean P Donegan, Edwin J Schwalbach, and Michael A Groeber. Zoning additive manufacturing process histories using unsupervised machine learning. *Materials Characterization*, 161:110123, 2020.
- [74] Shardul Kamat, Xuxiao Li, Benjamin Stump, Alex Plotkowski, and Wenda Tan. Multi-physics modeling of grain growth during solidification in electron beam additive manufacturing of inconel 718. *Modelling and Simulation in Materials Science and Engineering*, 31(1):015002, 2022.
- [75] William Halsey, James Ferguson, Alex Plotkowski, Ryan Dehoff, and Vincent Paquit. Geometry-independent microstructure optimization for electron beam powder bed fusion additive manufacturing. *Additive Manufacturing*, 35:101354, 2020.
- [76] Francis Ogoke and Amir Barati Farimani. Thermal control of laser powder bed fusion using deep reinforcement learning. *Additive Manufacturing*, 46:102033, 2021.
- [77] Benjamin Stump. An algorithm for physics informed scan path optimization in additive manufacturing. *Computational Materials Science*, 212:111566, 2022.
- [78] Yue Yang, John Billingham, Dragos Axinte, and Zhirong Liao. A rational approach to beam path planning in additive manufacturing: the inverse heat placement problem. *Proceedings of the Royal Society A*, 479(2270):20220386, 2023.
- [79] Benjamin Stump, Alex Plotkowski, and John Coleman. Solidification dynamics in metal additive manufacturing: analysis of model assumptions. *Modelling and Simulation in Materials Science and Engineering*, 29(3):035001, 2021.
- [80] Mahyar Khorasani, AmirHossein Ghasemi, Martin Leary, William O’Neil, Ian Gibson, Laura Cordova, and Bernard Rolfe. Numerical and analytical investigation on meltpool temperature of laser-based powder bed fusion of in718. *International journal of heat and mass transfer*, 177:121477, 2021.

- [81] Hrvoje Jasak, Aleksandar Jemcov, and Zeljko Tukovic. OpenFOAM: A C++ library for complex physics simulations. In *International workshop on coupled methods in numerical dynamics*, volume 1000, pages 1–20, 2007.
- [82] W. Bangerth, R. Hartmann, and G. Kanschat. deal.II—A general-purpose object-oriented finite element library. *ACM Trans. Math. Softw.*, 33(4):24–es, 2007.
- [83] TI DebRoy and SA David. Physical processes in fusion welding. *Reviews of modern physics*, 67(1):85, 1995.
- [84] Manyalibo J Matthews, Gabe Guss, Saad A Khairallah, Alexander M Rubenchik, Philip J Depond, and Wayne E King. Denudation of metal powder layers in laser powder bed fusion processes. *Acta Materialia*, 114:33–42, 2016.
- [85] Lu Wang, Yanming Zhang, and Wentao Yan. Evaporation model for keyhole dynamics during additive manufacturing of metal. *Physical Review Applied*, 14(6):064039, 2020.
- [86] Minglei Qu, Qilin Guo, Luis I Escano, Samuel J Clark, Kamel Fezzaa, and Lianyi Chen. Mitigating keyhole pore formation by nanoparticles during laser powder bed fusion additive manufacturing. *Additive Manufacturing Letters*, 3:100068, 2022.
- [87] C Panwisawas, CL Qiu, Y Sovani, JW Brooks, MM Attallah, and HC Basoalto. On the role of thermal fluid dynamics into the evolution of porosity during selective laser melting. *Scripta Materialia*, 105:14–17, 2015.
- [88] YS Lee and Wei Zhang. Modeling of heat transfer, fluid flow and solidification microstructure of nickel-base superalloy fabricated by laser powder bed fusion. *Additive Manufacturing*, 12:178–188, 2016.
- [89] Ying Yang, Dongdong Gu, Donghua Dai, and Chenglong Ma. Laser energy absorption behavior of powder particles using ray tracing method during selective laser melting additive manufacturing of aluminum alloy. *Materials & Design*, 143:12–19, 2018.
- [90] Jianchao Ye, Saad A Khairallah, Alexander M Rubenchik, Michael F Crumb, Gabe Guss, Jim Belak, and Manyalibo J Matthews. Energy coupling mechanisms and scaling behavior associated with laser powder bed fusion additive manufacturing. *Advanced Engineering Materials*, 21(7):1900185, 2019.
- [91] Kenneth C Mills. *Recommended values of thermophysical properties for selected commercial alloys*. Woodhead Publishing, 2002.
- [92] Shanping Lu, Hidetoshi Fujii, and Kiyoshi Nogi. Sensitivity of marangoni convection and weld shape variations to welding parameters in O<sub>2</sub>–Ar shielded GTA welding. *Scripta Materialia*, 51(3):271–277, 2004.
- [93] Y Wang and Hai-Lung Tsai. Effects of surface active elements on weld pool fluid flow and weld penetration in gas metal arc welding. *Metallurgical and Materials Transactions B*, 32:501–515, 2001.
- [94] S Mishra, TJ Lienert, MQ Johnson, and T DebRoy. An experimental and theoretical study of gas tungsten arc welding of stainless steel plates with different sulfur concentrations. *Acta Materialia*, 56(9):2133–2146, 2008.

- [95] T Mukherjee, V Manvatkar, A De, and T DebRoy. Dimensionless numbers in additive manufacturing. *Journal of Applied Physics*, 121(6):064904, 2017.
- [96] Gerry L Knapp, John Coleman, Matt Rolchigo, Miroslav Stoyanov, and Alex Plotkowski. Calibrating uncertain parameters in melt pool simulations of additive manufacturing. *Computational Materials Science*, 218:111904, 2023.
- [97] Jinghao Li, Xianglin Zhou, Mathieu Brochu, Nikolas Provatas, and Yaoyao Fiona Zhao. Solidification microstructure simulation of Ti-6Al-4V in metal additive manufacturing: A review. *Additive Manufacturing*, 31:100989, 2020.
- [98] Carolin Körner, Matthias Markl, and Johannes A. Koepf. Modeling and simulation of microstructure evolution for additive manufacturing of metals: A critical review. *Metallurgical and Materials Transactions A*, 51:4970–4983, 2020.
- [99] Joel Heang Kuan Tan, Swee Leong Sing, and Wai Yee Yeong. Microstructure modelling for metallic additive manufacturing: a review. *Virtual and Physical Prototyping*, 15(1):87–105, 2019.
- [100] Theofilos Gatsos, Karim A. Elsayed, Yuwei Zhai, and Diana A. Lados. Review on computational modeling of process–microstructure–property relationships in metal additive manufacturing. *JOM*, 72(1):403–419, 2020.
- [101] Wilfried Kurz, Michel Rappaz, and Rohit Trivedi. Progress in modelling solidification microstructures in metals and alloys. Part II: dendrites from 2001 to 2018. *International Materials Reviews*, 66(1):30–76, 2021.
- [102] Zhao Zhang, Yifei Wang, Peng Ge, and Tao Wu. A review on modelling and simulation of laser additive manufacturing: Heat transfer, microstructure evolutions and mechanical properties. *Coatings*, 12(9):1277, 2022.
- [103] Srikanth Bontha, Nathan W. Klingbeil, Pamela A. Kobryn, and Hamish L. Fraser. Effects of process variables and size-scale on solidification microstructure in beam-based fabrication of bulky 3D structures. *Materials Science and Engineering: A*, 513-514:311–318, 2009.
- [104] H. Yin and S.D. Felicelli. Dendrite growth simulation during solidification in the lens process. *Acta Materialia*, 58(4):1455–1465, 2010.
- [105] D Tourret, A Karma, A J Clarke, P J Gibbs, and S D Imhoff. Three-dimensional dendritic needle network model with application to al-cu directional solidification experiments. *IOP Conference Series: Materials Science and Engineering*, 84(1):012082, 2015.
- [106] D Tourret, L Sturz, A Viardin, and M Založnik. Comparing mesoscopic models for dendritic growth. *IOP Conference Series: Materials Science and Engineering*, 861(1):012002, 2020.
- [107] Joel Berry, Aurélien Perron, Jean-Luc Fattebert, John D. Roehling, Bey Vrancken, Tien T. Roehling, Debra L. Rosas, John A. Turner, Saad A. Khairallah, Joseph T. McKeown, and Manyalibo J. Matthews. Toward multiscale simulations of tailored microstructure formation in metal additive manufacturing. *Materials Today*, 51:65–86, 2021.
- [108] J G Pauza, W A Tayon, and A D Rollett. Computer simulation of microstructure development in powder-bed additive manufacturing with crystallographic texture. *Modelling and Simulation in Materials Science and Engineering*, 29(5):055019, 2021.

- [109] Anaïs Baumard, Danièle Ayrault, Olivier Fandeur, Cyril Bordreuil, and Frédéric Deschaux-Beaume. Numerical prediction of grain structure formation during laser powder bed fusion of 316 L stainless steel. *Materials & Design*, 199:109434, 2021.
- [110] Yigong Qin, Yuanxun Bao, Stephen DeWitt, Balasubramanian Radhakrishnan, and George Biros. Dendrite-resolved, full-melt-pool phase-field simulations to reveal non-steady-state effects and to test an approximate model. *Computational Materials Science*, 207:111262, 2022.
- [111] Tianju Xue, Zhengtao Gan, Shuheng Liao, and Jian Cao. Physics-embedded graph network for accelerating phase-field simulation of microstructure evolution in additive manufacturing. *npj Computational Materials*, 8(1):201, 2022.
- [112] L Kaufman and H Bernstein. *Computer calculation of phase diagrams with special reference to refractory metals*. Academic Press, New York, 1970.
- [113] Yimi Wang, Kangming Li, Frédéric Soisson, and Charlotte S. Becquart. Combining DFT and CALPHAD for the development of on-lattice interaction models: The case of Fe-Ni system. *Phys. Rev. Mater.*, 4:113801, 2020.
- [114] Trevor Keller, Greta Lindwall, Supriyo Ghosh, Li Ma, Brandon M. Lane, Fan Zhang, Ursula R. Kattner, Eric A. Lass, Jarred C. Heigel, Yaakov Idell, Maureen E. Williams, Andrew J. Allen, Jonathan E. Guyer, and Lyle E. Levine. Application of finite element, phase-field, and CALPHAD-based methods to additive manufacturing of Ni-based superalloys. *Acta Materialia*, 139:244–253, 2017.
- [115] Dovggy Bogdan, Simonelli Marco, and Pham Minh-Son. Alloy design against the solidification cracking in fusion additive manufacturing: an application to a FeCrAl alloy. *Materials Research Letters*, 9(8):350–357, 2021.
- [116] Rangasayee Kannan, Gerald L. Knapp, Peeyush Nandwana, Ryan Dehoff, Alex Plotkowski, Benjamin Stump, Ying Yang, and Vincent Paquit. Data mining and visualization of high-dimensional ICME data for additive manufacturing. *Integrating Materials and Manufacturing Innovation*, 11:57–70, 2022.
- [117] Rangasayee Kannan and Peeyush Nandwana. Thermodynamics and kinetics of precipitation and austenite reversion during aging of ti-free grade 300 maraging steel manufactured by laser powder bed fusion (LPBF). *Journal of Materials Science*, 56(33):18722–18739, 2021.
- [118] W Kurz, B Giovanola, and R Trivedi. Theory of microstructural development during rapid solidification. *Acta Metallurgica*, 34(5):823–830, 1986.
- [119] W Kurz and DJ Fisher. Dendrite growth at the limit of stability - tip radius and spacing. *Acta Metallurgica*, 29(1):11–20, 1981.
- [120] O Hunziker. Theory of plane front and dendritic growth in multicomponent alloys. *Acta Materialia*, 49(20):4191–4203, 2001.
- [121] K.A. Jackson and J.D. Hunt. Lamellar and rod eutectic growth. *Transactions of the Metallurgical Society of AIME*, 236(8):1129–&, 1966.
- [122] O Hunziker, M Vandyoussefi, and W Kurz. Phase and microstructure selection in peritectic alloys close to the limit of constitutional undercooling. *Acta Materialia*, 46(18):6325–6336, 1998.

- [123] S Fukumoto and W Kurz. Solidification phase and microstructure selection maps for Fe-Cr-Ni alloys. *ISIJ International*, 39(12):1270–1279, 1999.
- [124] JD HUNT. Steady-state columnar and equiaxed growth of dendrites and eutectic. *MATERIALS SCIENCE AND ENGINEERING*, 65(1):75–83, 1984.
- [125] M Gaumann, R Trivedi, and W Kurz. Nucleation ahead of the advancing interface in directional solidification. *Materials Science and Engineering A-Structural Materials Properties Microstructure and Processing*, 226:763–769, 1997. 9th International Conference on Rapidly Quenched and Metastable Materials, Bratislava, Slovakia, August 25-30, 1996.
- [126] Duyao Zhang, Arvind Prasad, Michael J. Bermingham, Carmelo J. Todaro, Michael J. Benoit, Mitesh N. Patel, Dong Qiu, David H. StJohn, Ma Qian, and Mark A. Easton. Grain refinement of alloys in fusion-based additive manufacturing processes. *Metallurgical and Materials Transactions A-Physical Metallurgy and Materials Science*, 51(9):4341–4359, 2020.
- [127] D. H. StJohn, M. Qian, M. A. Easton, and P. Cao. The interdependence theory: The relationship between grain formation and nucleant selection. *Acta Materialia*, 59(12):4907–4921, 2011.
- [128] M Gaumann, C Bezencon, P Canalis, and W Kurz. Single-crystal laser deposition of superalloys: Processing-microstructure maps. *Acta Materialia*, 49(6):1051–1062, 2001.
- [129] PA Kobryn and SL Semiatin. Microstructure and texture evolution during solidification processing of Ti-6Al-4V. *Journal of Materials Processing Technology*, 135(2-3):330–339, 2003. International Conference on Research and Development in Net-Shape Manufacturing, University of Birmingham, Birmingham, England, April 09-11, 2001.
- [130] W Kurz. Solidification microstructure processing maps: Theory and application. *Advanced Engineering Materials*, 3(7):443–452, 2001. EUROMAT 99 Meeting, Munich, Germany, September 27-30, 1999.
- [131] M. N. Patel, D. Qiu, G. Wang, M. A. Gibson, A. Prasad, D. H. StJohn, and M. A. Easton. Understanding the refinement of grains in laser surface remelted Al-Cu alloys. *Scripta Materialia*, 178:447–451, 2020.
- [132] Ingo Steinbach. Phase-field model for microstructure evolution at the mesoscopic scale. *Annual Review of Materials Research*, 43(1):89–107, 2013.
- [133] Z. Zhang, P. Ge, J. Y. Li, D. X. Ren, and T. Wu. Monte carlo simulations of solidification and solid-state phase transformation during directed energy deposition additive manufacturing. *Progress in Additive Manufacturing*, 7(4):671–682, 2022.
- [134] G. Boussinot, M. Doering, S. Hemes, O. Stryzhyboroda, M. Apel, and M. Schmidt. Laser powder bed fusion of eutectic Al-Ni alloys: Experimental and phase-field studies. *Materials & Design*, 198, 2021.
- [135] Chao Yang, Shilei Li, Xitao Wang, Junsheng Wang, and Houbing Huang. Phase-field simulation of multi-phase interactions in fe-c peritectic solidification. *Computational Materials Science*, 171:109220, 2020.
- [136] Ranadip Acharya, John A. Sharon, and Alexander Staroselsky. Prediction of microstructure in laser powder bed fusion process. *Acta Materialia*, 124:360–371, 2017.

- [137] Balasubramaniam Radhakrishnan, Sarma B. Gorti, John A. Turner, Ranadip Acharya, John A. Sharon, Alexander Staroselsky, and Tahany El-Wardany. Phase field simulations of microstructure evolution in IN718 using a surrogate Ni–Fe–Nb alloy during laser powder bed fusion. *Metals*, 9(1), 2019.
- [138] V. Fallah, M. Amoozrezaei, N. Provatas, S.F. Corbin, and A. Khajepour. Phase-field simulation of solidification morphology in laser powder deposition of ti–nb alloys. *Acta Materialia*, 60(4):1633–1646, 2012.
- [139] Tomohiro Takaki, Shinji Sakane, Munekazu Ohno, Yasushi Shibuta, Takashi Shimokawabe, and Takayuki Aoki. Primary arm array during directional solidification of a single-crystal binary alloy: Large-scale phase-field study. *Acta Materialia*, 118:230–243, 2016.
- [140] Shinji Sakane, Tomohiro Takaki, Roberto Rojas, Munekazu Ohno, Yasushi Shibuta, Takashi Shimokawabe, and Takayuki Aoki. Multi-GPUs parallel computation of dendrite growth in forced convection using the phase-field-lattice Boltzmann model. *Journal of Crystal Growth*, 474:154–159, 2017. The 8th International Workshop on Modeling in Crystal Growth.
- [141] Shinji Sakane, Tomohiro Takaki, Munekazu Ohno, Yasushi Shibuta, and Takayuki Aoki. Two-dimensional large-scale phase-field lattice boltzmann simulation of polycrystalline equiaxed solidification with motion of a massive number of dendrites. *Computational Materials Science*, 178:109639, 2020.
- [142] K. Reuther and M. Rettenmayr. Perspectives for cellular automata for the simulation of dendritic solidification – a review. *Computational Materials Science*, 95:213–220, 2014.
- [143] L Nastac. Numerical modeling of solidification morphologies and segregation patterns in cast dendritic alloys. *Acta Materialia*, 47(17):4253–4262, 1999.
- [144] W Wang, PD Lee, and M McLean. A model of solidification microstructures in nickel-based superalloys: predicting primary dendrite spacing selection. *Acta Materialia*, 51(10):2971–2987, 2003.
- [145] YH Shin and CP Hong. Modeling of dendritic growth with convection using a modified cellular automaton model with a diffuse interface. *ISIJ INTERNATIONAL*, 42(4):359–367, 2002.
- [146] M. F. Zhu, S. Y. Lee, and C. P. Hong. Modified cellular automaton model for the prediction of dendritic growth with melt convection. *Phys. Rev. E*, 69:061610, 2004.
- [147] Rui Chen, Qingyan Xu, and Baicheng Liu. A modified cellular automaton model for the quantitative prediction of equiaxed and columnar dendritic growth. *Journal of Materials Science & Technology*, 30(12):1311–1320, 2014.
- [148] Matthew R. Rolchigo, Michael Y. Mendoza, Peyman Samimi, David A. Brice, Brian Martin, Peter C. Collins, and Richard Lesar. Modeling of Ti-W solidification microstructures under additive manufacturing conditions. *Metallurgical and Materials Transactions A-Physical Metallurgy and Materials Science*, 48A(7):3606–3622, 2017.
- [149] Mohsen Asle Zaeem, Hebi Yin, and Sergio D. Felicelli. Comparison of cellular automaton and phase field models to simulate dendrite growth in hexagonal crystals. *Journal of Materials Science & Technology*, 28(2):137–146, 2012.

- [150] Damien Tournet and Alain Karma. Multi-scale needle-network model of complex dendritic microstructure formation. *IOP Conference Series: Materials Science and Engineering*, 33(1):012095, 2012.
- [151] D. Tournet and A. Karma. Multiscale dendritic needle network model of alloy solidification. *Acta Materialia*, 61(17):6474–6491, 2013.
- [152] Pierre-Antoine Geslin, Chih-Hung Chen, Amirhossein Molavi Tabrizi, and Alain Karma. Dendritic needle network modeling of the columnar-to-equiaxed transition. Part I: two dimensional formulation and comparison with theory. *Acta Materialia*, 202:42–54, 2021.
- [153] P.W. Liu, Y.Z. Ji, Z. Wang, C.L. Qiu, A.A. Antonysamy, L.-Q. Chen, X.Y. Cui, and L. Chen. Investigation on evolution mechanisms of site-specific grain structures during metal additive manufacturing. *Journal of Materials Processing Technology*, 257:191–202, 2018.
- [154] T. Isensee and D. Tournet. Convective effects on columnar dendritic solidification – a multiscale dendritic needle network study. *Acta Materialia*, 234:118035, 2022.
- [155] Santanu Paul, Jian Liu, Seth T. Strayer, Yunhao Zhao, Soumya Sridar, Michael A. Klecka, Wei Xiong, and Albert C. To. A discrete dendrite dynamics model for epitaxial columnar grain growth in metal additive manufacturing with application to inconel. *Additive Manufacturing*, 36:101611, 2020.
- [156] Wenda Tan and Yung C. Shin. Multi-scale modeling of solidification and microstructure development in laser keyhole welding process for austenitic stainless steel. *Computational Materials Science*, 98:446–458, 2015.
- [157] Neil Bailey and Yung Shin. Multi-track, multi-layer dendrite growth and solid phase transformation analysis during additive manufacturing of H13 tool steel using a combined hybrid cellular automata/phase field, solid-state phase prediction models. *The International Journal of Advanced Manufacturing Technology*, 120, 2022.
- [158] X.X. Yao, P. Ge, J.Y. Li, Y.F. Wang, T. Li, W.W. Liu, and Z. Zhang. Controlling the solidification process parameters of direct energy deposition additive manufacturing considering laser and powder properties. *Computational Materials Science*, 182:109788, 2020.
- [159] Ch.-A Gandin and M Rappaz. A 3D cellular automaton algorithm for the prediction of dendritic grain growth. *Acta Materialia*, 45(5):2187–2195, 1997.
- [160] Xuxiao Li and Wenda Tan. Numerical investigation of effects of nucleation mechanisms on grain structure in metal additive manufacturing. *Computational Materials Science*, 153:159–169, 2018.
- [161] A. Zinoviev, O. Zinovieva, V. Ploshikhin, V. Romanova, and R. Balokhonov. Evolution of grain structure during laser additive manufacturing. simulation by a cellular automata method. *Materials & Design*, 106:321–329, 2016.
- [162] O. Zinovieva, A. Zinoviev, V. Romanova, and R. Balokhonov. Three-dimensional analysis of grain structure and texture of additively manufactured 316l austenitic stainless steel. *Additive Manufacturing*, 36:101521, 2020.
- [163] Mohammad Sadegh Mohebbi and Vasily Ploshikhin. Implementation of nucleation in cellular automaton simulation of microstructural evolution during additive manufacturing of Al alloys. *Additive Manufacturing*, 36:101726, 2020.

- [164] Omar Lopez-Botello, Uriel Martinez-Hernandez, José Ramírez, Christophe Pinna, and Kamran Mumtaz. Two-dimensional simulation of grain structure growth within selective laser melted AA-2024. *Materials & Design*, 113:369–376, 2017.
- [165] Yanping Lian, Zhengtao Gan, Cheng Yu, Dmitriy Kats, Wing Kam Liu, and Gregory J. Wagner. A cellular automaton finite volume method for microstructure evolution during additive manufacturing. *Materials & Design*, 169:107672, 2019.
- [166] Javed Akram, Pradeep Chalavadi, Deepankar Pal, and Brent Stucker. Understanding grain evolution in additive manufacturing through modeling. *Additive Manufacturing*, 21:255–268, 2018.
- [167] Dong-Rong Liu, Shuhao Wang, and Wentao Yan. Grain structure evolution in transition-mode melting in direct energy deposition. *Materials & Design*, 194:108919, 2020.
- [168] Johannes A. Koepf, Martin R. Gotterbarm, Matthias Markl, and Carolin Körner. 3D multi-layer grain structure simulation of powder bed fusion additive manufacturing. *Acta Materialia*, 152:119–126, 2018.
- [169] J.A. Koepf, D. Soldner, M. Ramsperger, J. Mergheim, M. Markl, and C. Körner. Numerical microstructure prediction by a coupled finite element cellular automaton model for selective electron beam melting. *Computational Materials Science*, 162:148–155, 2019.
- [170] Matt Rolchigo, Samuel Temple Reeve, Benjamin Stump, Gerald L. Knapp, John Coleman, Alex Plotkowski, and James Belak. Exaca: A performance portable exascale cellular automata application for alloy solidification modeling. *Computational Materials Science*, 214:111692, 2022.
- [171] Sumair Sunny, Haoliang Yu, Ritin Mathews, Arif Malik, and Wei Li. Improved grain structure prediction in metal additive manufacturing using a dynamic kinetic monte carlo framework. *Additive Manufacturing*, 37:101649, 2021.
- [172] Theron M. Rodgers, Daniel Moser, Fadi Abdeljawad, Olivia D. Underwood Jackson, Jay D. Carroll, Bradley H. Jared, Dan S. Bolintineanu, John A. Mitchell, and Jonathan D. Madison. Simulation of powder bed metal additive manufacturing microstructures with coupled finite difference-monte carlo method. *Additive Manufacturing*, 41:101953, 2021.
- [173] Z. Zhang, Z.J. Tan, X.X. Yao, C.P. Hu, P. Ge, Z.Y. Wan, J.Y. Li, and Q. Wu. Numerical methods for microstructural evolutions in laser additive manufacturing. *Computers & Mathematics with Applications*, 78(7):2296–2307, 2019. Simulation for Additive Manufacturing.

